DEVELOPMENT OF A PORTABLE NITRITE SENSOR USING COLORIMETRIC AND ELECTROCHEMICAL PLATFORM ON A SINGLE DEVICE

By

MISS Parima TIAWPISITPONG

A Thesis Submitted in Partial Fulfillment of the Requirements

for Master of Science CHEMISTRY

Department of CHEMISTRY

Silpakorn University

Academic Year 2023

การพัฒนาเซ็นเซอร์ตรวจวัดไนไตร์ทพกพา ด้วยการตรวจวัดสี และเทคนิคทางเคมีไฟฟ้าบนอุปกรณ์ชิ้นเดียว

โดย
นางสาวพริมา เตียวไพสิฐพงษ์

วิทยานิพนธ์นี้เป็นส่วนหนึ่งของการศึกษาตามหลักสูตรวิทยาศาสตรมหาบัณฑิต
สาขาวิชาเคมี แผน ก แบบ ก 2
ภาควิชาเคมี
มหาวิทยาลัยศิลปากร
ปีการศึกษา 2566

DEVELOPMENT OF A PORTABLE NITRITE SENSOR USING COLORIMETRIC AND ELECTROCHEMICAL PLATFORM ON A SINGLE DEVICE

By

MISS Parima TIAWPISITPONG

A Thesis Submitted in Partial Fulfillment of the Requirements

for Master of Science CHEMISTRY

Department of CHEMISTRY

Academic Year 2023

Title	Development of a portable nitrite sensor using colorimetric and electrochemical platform on a single device
By	MISS Parima TIAWPISITPONG
Field of Study	CHEMISTRY
Advisor	Assistant Professor Dr. Kanokwan Charoenkitamorn

Faculty of Science, Silpakorn University in Partial Fulfillment of the Requirements for the Master of Science

.....Dean of Faculty of Science
(Assistant Professor Dr. Narong Chimpalee)

Approved by

.....Chair person
(Dr. Sudkate Chaiyo)

.....Advisor
(Assistant Professor Dr. Kanokwan Charoenkitamorn)

.....Committee
(Assistant Professor Dr. Sumonmarn Chaneam)

.....External Examiner
(Dr. Sudkate Chaiyo)

640720001 : Major CHEMISTRY
Keyword : nitrite, dual-mode detection, colorimetry, electrochemistry

MISS Parima TIAWPISITPONG : Development of a portable nitrite sensor using colorimetric and electrochemical platform on a single device Thesis advisor : Assistant Professor Dr. Kanokwan Charoenkitamorn

The dissertation focused on the development of a portable nitrite sensor using colorimetric and electrochemical platforms on a single device. Nitrite is commonly used as food coloring and preservation in processed food and is present in natural agricultural products. Despite its widespread use, inappropriate application and potential health risks underscore a significant concern for public safety. To address this issue and ensure the well-being of citizens, a proposed solution involves the development of a portable nitrite sensor for on-site applications. This innovative device integrates a pre-screening feature utilizing a colorimetric paper-based analytical device (PAD) and a highly sensitive quantitative analysis employing electrochemical detection. The colorimetric detection on the PAD involves a decolorization process of potassium permanganate ($KMnO_4$) under acidic conditions to identify nitrite. The resulting color change is then correlated with a color chart, providing an approximation of the nitrite concentration in the sample. Simultaneously, the electrochemical sensor, incorporating a cellulose acetate (CA) modified screen-printed carbon electrode, is strategically positioned beneath the colorimetric PAD. This setup also allows for a more sensitive quantitative analysis of nitrite, with the nitrite oxidation process depicted through the differential pulse voltammogram (DPV) at +0.800 V vs Ag/AgCl. This dual-mode approach aims to offer a practical and efficient solution for the rapid detection and quantification of nitrite and, a variety of applications through accessibility to general users and specialists. Furthermore, the test can be easily and widely applied to samples. This is particularly useful when the samples possess a color that could potentially affect the colorimetric analysis.

ACKNOWLEDGEMENTS

I am deeply grateful to my advisor, Asst. Prof. Kanokwan Charoenkitamorn, for her strong support and guidance throughout my master's program. Her expertise and patience have been invaluable to me and have played a crucial role in the success of this thesis.

I would like to thank the Faculty of Science, Silpakorn University, for the Faculty of Science, Silpakorn University, grant number SRIF-PRG-2566-04, and the Development and Promotion of Science and Technology Talents Project (DPST) for the graduate scholarship.

Finally, I am also grateful to thank Asst. Prof. Sumonmarn Chaneam and Dr. Sudkate Chaiyo for serving on my thesis committee and providing valuable feedback and suggestions.

Parima TIAWPISITPONG

TABLE OF CONTENTS

Page

LIST OF TABLES

Page

LIST OF FIGURES

Page

CHAPTER I:

INTRODUCTION

1.1 Introduction

Nitrite has found extensive usage in both industrial and agricultural sectors and is also prevalent in food, water, biological systems, and the environment. It is mostly used in processed meats as a color stabilizer and preservative agent. Preservation through nitrite addition involves inhibiting the growth of pathogens and enhancing the shelf life by preserving the color of the food product. Also, nitrite can be broken down to nitric oxide (NO), which reacts with myoglobin (Mb) to create a stable pink color [1], preventing the development of undesirable brown hues and maintaining the characteristic color of cured meats. While this chemical possesses powerful properties, excessive exposure to it increases the risk of cancer and methemoglobinemia. Nitrite spontaneously converts to nitrosating agents and subsequently reacts with amine compounds resulting in primary nitrosamines which further decompose into a diazonium compound, a DNA alkylating agent that results in DNA damage, a causal factor for cancer development [2]. In the case of methemoglobinemia effect on infants and laboratory animals, an oxygen deficiency state, hemoglobin can be oxidized by nitrite and form methemoglobin which loses validity to bind with oxygen.

In the agriculture industry, nitrite serves as an important intermediate compound in the nitrogen cycle. Nitrogen-based fertilizers, such as ammonium-based and nitrate-based fertilizers, when applied, undergo microbial transformations that can lead to the accumulation of nitrite in the environment. The negative effects of excessive nitrite on environmental microorganisms have

been well-reported [3-5]. High levels of nitrite in the environment can disrupt the balance of the ecosystem, leading to an imbalance in the system. Elevated nitrite levels in water bodies are identified as a significant contributor to water pollution. This phenomenon provides a harmful effect on aquatic ecosystems as it results in oxygen depletion which poses a threat to aquatic life [6, 7]. The possibility of overdose nitrite exposure is irresistible.

Although it has widespread applications, it poses a threat as a toxic inorganic contaminant, presenting hazards to human health and other organisms. Monitoring nitrite levels helps assess the health of ecosystems and prevents potential adverse effects on water quality and biodiversity. Relevant organizations have set the limit of nitrite concentration in foodstuffs to encourage hygiene standards. According to The World Health Organization (WHO) announcement, the defined levels of nitrite are 0.06 mg/kg of body weight/ day in food additives [8], and 3 mg/L in drinking water [9] respectively.

In recent years, numerous approaches have been suggested for the detection and monitoring of nitrites such as spectrophotometry [10-15], chromatography [16-20], and capillary electrophoresis [21-24]. Despite achieving satisfactory levels of sensitivity, accuracy, repeatability, and reproducibility, certain limitations continue to hinder various methods used for determining nitrite levels in food, environmental samples, and human bodies. These challenges include immobility, specific expertise requirements, and the need for expensive equipment. However, colorimetric detection has emerged as a popular and simple alternative, as color changes can be identified by the naked eye. Among the various protocols used for this approach, the Griess reagent is the most widely used and traditional system. This assay is related to two subsequent reactions. First, sulfanilamide reacts with nitrite in acidic media by diazotization reaction, generating diazonium salt which respectively reacts with *N*-(1-Naphthyl)-ethylenediamine in an azo coupling reaction, forming an azo dye, noticed pink-red color in products by the

naked eye and providing maximum absorbance at wavelength 540 nm. The overview of the Griess reaction is shown in Figure 1.

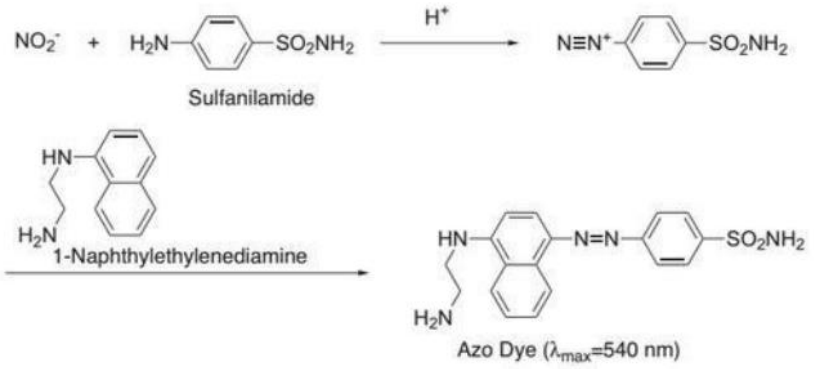

Figure 1 Griess reactions for colorimetric detection of nitrite/nitrate assay kit [25]

The Griess reaction is a convenient method for colorimetric detection, which involves monitoring the color change of an azo dye with the naked eye. However, when dealing with samples that are already colored, the color of the sample can interfere with the detection of nitrite, leading to inaccurate results. Additionally, the Griess reagent is costly and can only be purchased through chemical suppliers. As a widely available and reasonably priced reagent for the colorimetric technique, potassium permanganate ($KMnO_4$) is being considered as an alternative to increase the accessibility of this simple method. The redox reaction between nitrite and $KMnO_4$ with sulfuric acid (H_2SO_4) acidified solution is shown in equation 1.

$$2KMnO_4 + 3H_2SO_4 + 5NaNO_2 \longrightarrow 2MnSO_4 + K_2SO_4 + 5NaNO_3 + 3H_2O \quad (1)$$

The purple color of $KMnO_4$ fades when nitrite is present. $KMnO_4$ can be used as an alternative reagent for the semi-quantitative determination of nitrite, but it may not be sensitive enough for trace amounts. Furthermore, the color of samples could alter the faded color of $KMnO_4$. Therefore, relying solely on colorimetric detection is suitable for semi-quantitative analysis but insufficient for quantitative analysis.

Electrochemical detection is a method that offers high sensitivity and precision in determining the concentration of nitrite in samples. A portable electrochemical device with a microscale screen-printed electrode (SPE) design is available nowadays, which allows for portability and suitable on-field testing. Nitrite can undergo an oxidation reaction as shown in equation 2, which produces a current signal that can be used to determine its concentration.

$$NO_2^- + H_2O \longrightarrow NO_3^- + 2H^+ + 2e^- \quad (2)$$

With electrochemical detection, the sensor can achieve quantitative analysis with sensitivity and unaffected by the color of the samples.

In this work, our group has proposed a portable sensor by gathering the benefits of both colorimetric and electrochemical detections in a single device. The semi-quantitative of nitrite by colorimetric detection has been combined with the quantitative electrochemical detection to achieve the wide ability of the nitrite sensor. The estimated concentration of nitrite relies on the redox reaction of acidified purple permanganate in the presence of nitrite, resulting in the faded reagent color correlated with the concentration of nitrite as shown in equation 3.

$$2MnO_4^- + 5NO_2^- + 6H^+ \longrightarrow 2Mn^{2+} + 5NO_3^- + 3H_2O \quad (3)$$

In part of the quantitative analysis of nitrite by electrochemical detection, the oxidation of nitrite on the electrode surface is expected to be the same as above mentioned in equation 2.

The proposed sensor combines both colorimetric and electrochemical detection in a single device. The device has two sections: a colorimetric paper pad with acidified $KMnO_4$ reagent and an electrode pad of cellulose acetate-modified screen-printed carbon electrode (CA/SPCE) for electrochemical detection. The device can display both semi-quantitative and quantitative determination of nitrite at the same time by allowing fluid to penetrate paper through the surface of the electrode. For colorimetric detection, a phone camera

was used to collect experimental data. The color intensity including red, green, blue, and weighting greyscale was measured by ImageJ. Underneath the colorimetric paper, the anodic current of nitrite was conducted using an electrochemical transducer. To improve the sensitivity of electrochemical detection, cellulose acetate was modified on a screen-printed carbon electrode (SPCE). The current signal on the anodic peak at +0.70 V vs Ag/AgCl ink approximately by DPV, expressing the oxidation process of nitrite was indicated for quantitative analysis of nitrite. For this reason, the proposed dual-mode sensor serves not only to provide advantages such as swift response, cost-effectiveness, extended analytical range, and portability but also broadens customer acquisition to both inexperienced and experienced users. This enhances the accessibility of nitrite detection, making it easier for users to access affordable reagents and common equipment.

1.2 Objectives of the thesis

There are two purposes of this dissertation.

1) To invent a low-cost dual electrochemical and colorimetric sensing platform of nitrite sensor from cellulose acetate modified on SPCE with topped-up with the colorimetric microfluidic paper.
2) To apply a fabricated sensor for nitrite determination in real samples such as food and environment samples.

1.3 Scope of the thesis

According to purposes, the portable proposed sensor was custom-designed and fabricated in a single device. To obtain the best efficiency, the optimization of relevant parameters was investigated. For colorimetric detection, the interested condition includes supporting electrolytes and pH, the concentration of reagent, drying time, and reaction time. For electrochemical detection, the various types of materials were carefully selected and modified on the electrode transducer. For optimization of the electrochemical parameters, supporting electrolytes and pH, the

amount of modifier, and DPV parameters were studied. Characteristics of the fabricated sensor, morphology, and electrochemical behavior of the electrode surface were investigated.

Eventually, the combination of optimized conditions on both colorimetric and electrochemical detection, the analytical performance including linear range, limit of detection, accuracy, and precision was studied. To prove the possibility of the proposed sensor, interferences, method validation, and utilization in real samples were demonstrated.

1.4 Research utilization

1) Obtain the dual-mode electrochemical and colorimetric sensing mode of the nitrite sensor.
2) Succeed in improving both colorimetric and electrochemical performance in terms of sensitivity, accuracy, portability, and simplicity for the determination of nitrite.
3) Succeed in applying the proposed sensor in food and environmental samples.

This dissertation includes five chapters. Chapter I is an introduction that exhibits an overview of the dissertation. Chapter II is a theory that describes the fundamentals of colorimetric and electrochemical detection, and also includes the related literature reviews of the previous study on the detection of nitrite. Chapter III contains an experiment section, referring to all chemicals, reagents, and instruments used to detect nitrites as well as the procedure for the measurement. Chapter IV, results and discussion, of the proposed sensor that applies for determination of nitrite. Chapter V is a conclusion and future perspectives.

CHAPTER II:

THEORY AND LITERATURE REVIEWS

2.1 Analyte: Nitrite (NO_2^-)

The chemical formula of the nitrite ion is NO_2^-, which consists of one nitrogen atom (N) and two oxygen atoms (O), arranged in a bent shape as shown in Figure 2. The nitrite ion exhibits a symmetrical structure (C2v symmetry), where both N–O bonds possess equal length, and the bond angle is approximately 115°. According to valence bond theory, it is exhibited as a resonance hybrid with equal contributions from two mirror-image canonical forms in Figure 3. In molecular orbital theory, there exists a sigma bond between each oxygen atom and the nitrogen atom, along with a delocalized pi bond formed from the p-orbitals on nitrogen and oxygen, oriented perpendicular to the molecular plane. The negative charge of the ion is evenly distributed over the two oxygen atoms. Both the nitrogen and oxygen atoms carry a lone pair of electrons, classifying the nitrite ion as a Lewis base.

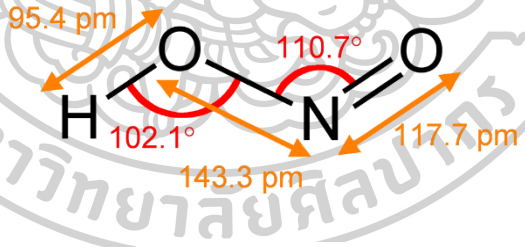

Figure 2 Chemical structure of nitrite

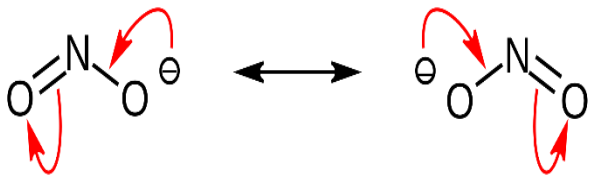

Figure 3 The resonance hybrid for NO_2^-

This ion can be found generally in nature and food industries. In nature, the nitrite anion serves as a common intermediate in the nitrogen cycle, playing a pivotal role in the conversion of ammonia (NH_3) to nitrate (NO_3^-) as shown in Figure 4. Ammonia is excreted by piscine life respiration and waste during the initial stages of the cycle. Nitrifying bacteria, such as nitrosomonas and nitrosococcus, convert NH_3 to NO_2^-, subsequently converted into nitrate by another bacteria [26, 27].

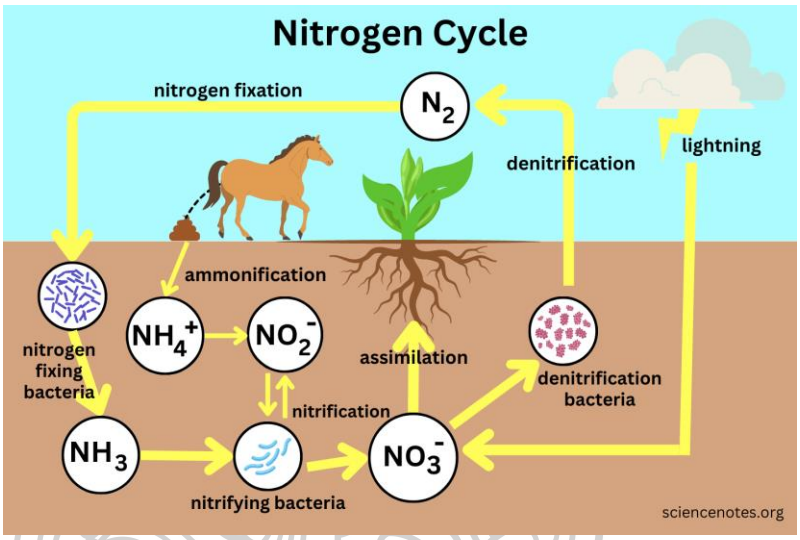

Figure 4 Nitrogen cycle-figure [28].

In the food industries, nitrites, commonly in the form of sodium nitrite ($NaNO_2$), serve critical functions as both preservatives and colorants in processed meat products. Their primary use lies in preserving cured meats such as bacon, ham, sausages, and hot dogs. Nitrites play a crucial role in preventing the growth of harmful bacteria, particularly *Clostridium botulinum*, which can lead to botulism, a potentially life-threatening foodborne illness. Additionally, nitrite functions as a color-fixing agent, contributing to the distinctive pink or reddish color observed in cured meats. The interaction of nitrite with myoglobin, a protein responsible for meat color, results in the formation of a stable pink pigment known as nitrosomyoglobin. This process enhances the visual appeal of processed meats. However, it's important to note that while nitrite provides these benefits, their excessive consumption has been linked to health concerns. The formation of nitrosamines, potentially carcinogenic compounds, is a risk associated with excessive nitrite intake [2].

To address these concerns, regulations, and guidelines are implemented in the food industry to limit the level of nitrite allowed in food products. The World Health Organization (WHO) has defined specific levels for nitrite intake, such as 0.06 mg/kg of body weight/day in food additives [8] and 3 mg/L in drinking water [9]. These regulatory measures aim to ensure the safe and controlled use of nitrites in the food industry, balancing their beneficial preservative and color-enhancing properties with health considerations.

2.2 Colorimetry

The ability to perceive colors is among the earliest skills acquired by humans, as individuals learn to distinguish various shades and intensities of color from an early age. In the realm of chemistry, color holds significant importance and is extensively utilized. Early in the evolution of chemistry, scientists observed that alterations in the color of a solution signaled the taking place of a chemical reaction. Moreover, they noted that the intensity of color could be correlated with the concentration of the products involved in that reaction. This observation predates the formalization of any color vision theory, and the utilization of selective colorimetric reactions has emerged as a potent tool for qualitative analysis. Therefore, colorimetry refers to the scientific technique used to measure concentration based on the intensity of color appearance.

Compared with other methods, the colorimetric method has some obvious advantages, such as low cost, simple instruments (or, in the case of naked eye detection, no instruments), and can be qualitatively or semi-qualitatively identified by the naked eye. However, colorimetry is generally less sensitive.

2.2.1 Fundamental of colorimetry

Colorimetry, in the realms of physics and chemistry, pertains to the assessment of the optical density (wavelength and intensity) of electromagnetic radiation within the visible region. It has been used historically to determine the concentration of colored compounds in a solution. The intensity of the detected signal is proportional to the colored solution concentration as illustrated in Figure 5.

Figure 5 A typical equation for direct colorimetry expresses the relationship between substrate concentration and the color signal [29].

When the absorbance of light is employed, the concentration of luminescence species is proportional to absorbance according to the Beer-Lambert law [30].

In alignment with the contemporary trends in analytical chemistry, there is a notable emphasis on the development of straightforward, cost-effective, environmentally friendly analytical methods. These methods aim to minimize sample volume and reagent usage, reduce chemical waste generation, and incorporate data acquisition through digital imaging. This emphasis on simplicity, affordability, and sustainability reflects the evolving priorities in the field. The cost-effective substrate material, characterized by a high surface area to volume ratio, is the fibrous network of paper cellulose and similar porous hydrophilic materials [31]. This structure provides benefits such as power-free fluid transport, enhancing the capacity to absorb reagents, and improving detection limits in colorimetric methods.

Nowadays, the colorimetric reaction commonly operates on paper-based analytical devices (PADs) involving the measurement of the color intensity from the surface of a testing zone. Image capturing for quantification can be achieved using a scanner, smartphone, or digital camera. These color spaces are typically managed by various processing software, including Adobe Photoshop, Image J, Photometrix, and Image Color Picker. Among these software types, Image J is an open-source Java image processing tool widely employed for handling images obtained from digital

devices. The captured image can be decomposed into RGB channels and converted to grayscale for each pixel. This is done by selecting the sample reaction zone or region of interest (ROI), which is identified as the location containing the reaction color product. The colorimetric reaction signal is then extracted from this selected area [32-34]. To quantify the results, the color intensity is then compared to a calibration curve.

2.2.2 RGB color specification system in ImageJ software

In a color mixture system, once the color matching functions have been determined, the tristimulus specification of any arbitrary color stimulus can be determined easily. However, standardization is necessary to be able to compare results because the color-matching functions depend on the basic and reference stimuli. In 1931, Commission Internationale de L'Eclairage (CIE) designed CIE 1931 RGB color space as standard color matching functions, the mathematic relationships occurred between the distributions of wavelengths across the electromagnetic visible spectrum and the colors perceived through physiological processes in human vision. The RGB color model is based on the additive color theory, where different combinations of red, green, and blue light are mixed to create a wide range of colors [35, 36]. This model is widely used in electronic devices such as computer monitors, televisions, and digital cameras.

In ImageJ, the RGB color specification system refers to the representation of colors as 24 bits-RGB image, which leaves 8 bits in each red, green, and blue color component. Each pixel in an image is defined by the intensity levels of each color component. These intensity values range from 0 to 255 for each color channel, where 0 represents no intensity (black) and 255 represents maximum intensity (full color) [37].

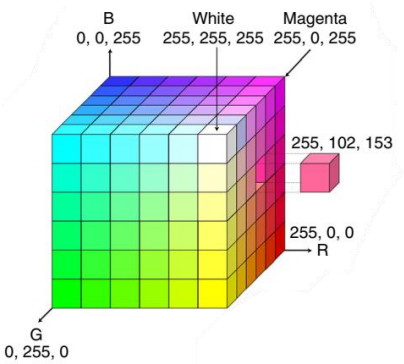

Figure 6 Simplified RGB Color spaces [38].

ImageJ allows users to view and manipulate images in RGB color space. Users can adjust the intensity levels of individual color channels to modify the appearance of the image. Additionally, ImageJ provides tools for converting images between different color spaces, such as RGB and grayscale. The average method of grayscale is an average intensity of red, green, and blue color as described in equation 4.

$$\text{Unweighed grayscale} = \frac{(R+G+B)}{3} \quad (4)$$

Even though the conventional average method is simple, it doesn't work as well as expected due to it assigns equal weight to each color component. But human eyes respond differently to various colors. Specifically, eyes display greater sensitivity to green, followed by red, and finally blue. Thus, the grayscale should be weighed proportionally to each component, which can be described as equation 5.

$$\text{Weighed grayscale} = \frac{(0.3\text{R}) + (0.59\text{G}) + (0.11\text{B})}{3} \quad (5)$$

Where R = the mean average intensity of red color.

G = the mean average intensity of green color.

B = the mean average intensity of blue color.

In this dissertation, the colorimetric detection method for determining nitrite was employed using colorimetric PADs. The captured images were processed using a smartphone. The ImageJ software was used for RGB model color analysis resulting in

histograms. The mean intensities of red, green, blue, and weighed grayscale were recorded.

2.3 Electrochemistry

In general, there are two types of electrochemical cells: galvanic cells and electrolytic cells. A galvanic cell generates an electric current through the energy released in a spontaneous redox reaction. Conversely, an electrolytic cell requires an external source of electrical energy to drive a chemical reaction. The electrolytic method boasts several advantages, including high sensitivity with a broad linear dynamic range for both inorganic and organic species, simplicity, rapid analysis time, and the ability to simultaneously detect various target analytes. The choice of electrochemical techniques depends on the nature of the ions or compounds of interest and their potential interferences in the surrounding environment [39].

Electrochemistry is a valuable tool for studying the oxidation or reduction that a material undergoes during electrical stimulation. These redox reactions, encompassing both reduction and oxidation, can offer insights into the concentration, reaction mechanisms, kinetics, chemical status, and other behaviors of a species in a solution.

2.3.1 Fundamentals of electrochemistry

In controlled-potential electrochemical experiments, the objective is to measure the current, which is correlated with the concentration of target analytes. To achieve this aim, the transfer of electrons at the transducer surface during the redox reaction of the analyte was monitored [39-43].

$$O + ne^- \rightleftharpoons R \quad (6)$$

Where O and R are the oxidized and reduced species, respectively, of a redox reaction, n is the number of electrons that are involved. The redox reaction occurs in

the potential region where the electron transfer is favorable thermodynamically or kinetically. For the thermodynamically controlled system, the activities of the electroactive oxidized and reduced form can be established by the potential of the electrode according to the Nernst equation.

$$E = E^0 - \frac{2.3026RT}{nF} log_{10} \frac{C_R(0,t)}{C_O(0,t)} \quad (7)$$

Where E^0 = standard potential for the redox reaction.

R = universal ideal gas constant (8.314 $JK^{-1}mol^{-1}$).

T = temperature in kelvins.

n = number of e^- (electron) transfer in redox reaction.

F = Faraday constant (96,487 coulombs).

$C_R(0,t)$ = concentration of the reduced form.

$C_O(0,t)$ = concentration of the oxidized form.

2.3.2 Mass transfer-controlled reaction

In electrochemistry, a mass transfer-controlled reaction refers to a situation where the rate of a chemical reaction is primarily determined by the transport of reactants or products to or from the electrode surface.

There are three basic mechanisms of mass transport as described.

2.3.2.1 Diffusion

Diffusion is defined as the process by which ions or molecules move randomly from regions of higher concentration (bulk) to regions of lower concentration (electrode interface). The velocity at which a molecule undergoes diffusion relies on the disparity in concentration between two points within the solution, denoted as the concentration gradient. It is also contingent upon the diffusion coefficient, D, a characteristic value for a specific species in the solution at a constant temperature. Fick's first law describes the movement of a chemical species influenced by a concentration gradient. For particle i, diffusion through a cross-

sectional area is a function of the concentration gradient across the selected area. The flux, denoted as J_i, representing particles per unit time across the specified segment, is expressed as follows:

$$J_i = -D_i \frac{\partial C_i}{\partial x} \quad (8)$$

Here, $\frac{\partial C_i}{\partial x}$ signifies the concentration gradient, and D_i is the diffusion coefficient for the particle.

2.3.2.2 Migration

Migration refers to the movement of charged species (ions) in response to an electric field. Positively charged ions move toward the negatively charged electrode (cathode), and negatively charged ions move toward the positively charged electrode (anode). The influence of migration on the overall flux is directly proportional to the ion's charge, ion concentration, diffusion coefficient, and the strength of the electric field gradient experienced by the ion.

2.3.2.3 Convection

Convection involves the bulk movement of electrolytes, carrying ions or molecules along with it. This movement is typically driven by external forces such as stirring or fluid flow. The stirring rate of a solution is typically manageable, and the convective component (in a single dimension) of the total flux of a species can be elucidated by its hydrodynamic velocity.

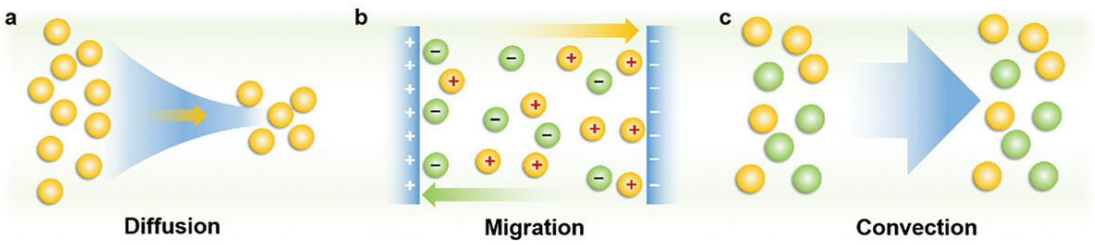

Figure 7 Three basic mechanisms of mass transport [44].

2.3.3 Voltammetry

Voltammetry represents a category of electrochemical methods used in analytical chemistry for both qualitative and quantitative analysis. This technique involves applying varying potentials to an electrode surrounded by a supporting electrolyte containing electro-active species and measuring the resulting current response through the electrode. A typical voltammetric electrochemical cell comprises either three or two electrodes, including the working electrode (WE), reference electrode (RE), and an optional counter electrode (CE). The working electrode is where the redox reaction takes place, making it crucial for signal responses to analytes. The reference electrode maintains a constant potential, as no electron flow occurs through it. The counter electrode, if present in a three-electrode system, allows an electrical current from reactions other than those at the working electrode. The working electrode undergoes a variable potential excitation signal, leading to changes in its potential corresponding to the constant potential of the reference electrode. This process provides valuable information about the analyte being analyzed. The measured current flow between the working electrode and reference electrode as a function of the applied potential is referred to as a "voltammogram." Figure 8 illustrates the excitation waveform employed in various voltammetry techniques and the corresponding voltammogram.

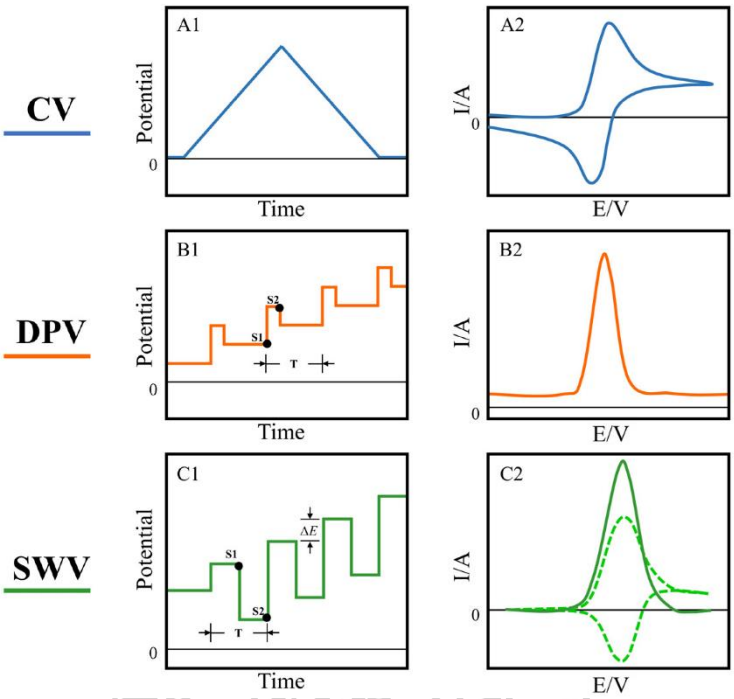

Figure 8 Illustration of the excitation waveform employed in various voltammetry techniques and the corresponding voltammogram [45].

In this dissertation, cyclic voltammetry (CV) was applied for electrochemical behavior study. Differential pulse voltammetry (DPV) was utilized for the quantitative electrochemical detection of NO_2^-.

2.3.3.1 Cyclic Voltammetry (CV)

CV involves a triangular or sawtooth waveform as the excitation signal. The potential is swept forward and backward in a cyclic potential as shown in Figure 8. This technique provides information about the reversibility and kinetics of electrochemical reactions.

For reversible redox reactions, the anticipated voltammogram in a single potential cycle is depicted in Figure 9. Initially, it was assumed that only the oxidized form (O) was present. Therefore, the first half-cycle is scanned in the negative scan of potential, where no reduction takes place. As the potential approaches the characteristic E^0 for the redox process, an increase in cathodic current

is observed until it reaches a peak. Throughout this phase, the reduced form (R) is generated near the electrode surface. After the potential traverses at least 90/n mV beyond the cathodic peak, the direction is reversed, initiating the reduction of the R process. The maximum anodic and cathodic peak currents, denoted as i_{pa} and i_{pc}, are measured by baseline extrapolation, as illustrated in the voltammogram in Figure 9. The values E_{pc} and E_{pa} indicate the cathodic and anodic peak potentials at which cathodic peak current (i_{pc}) and anodic peak current (i_{pa}) are acquired, respectively. The peak current (i_p) for a reversible process is determined by the Randles-Sevcik equation.

$$i_p = (2.69 \times 10^5) n^{3/2} A C D^{1/2} v^{1/2} \quad (8)$$

where n = number of electrons

A = electrode area (cm^2)

C = concentration ($mol\ cm^{-3}$)

D = diffusion coefficient ($cm^2\ s^{-1}$)

v = scan rate ($V\ s^{-1}$)

The Randles-Sevcik equation states that i_p is a scan root of the scan rate and is directly proportional to the analyte concentration. Therefore, it is possible to demonstrate the mass-transfer process of electroactive species towards the electrode surface using the linear relationship between i_p and scan root scan rate. The formal potential (E^0) of the redox process is connected to Ep. E^0 is situated in the middle of the reversible process, between E_{pa} and E_{pc}.

$$E^0 = \frac{E_{pa} + E_{pc}}{2} \quad (9)$$

The separation of peak potential for the reversible process is calculated as shown in Equation 10. The number of electrons (n) transferred in the reversible redox process can be determined as a criterion for Nernstian behavior.

$$\Delta E_p = E_{pa} - E_{pc} = \frac{5.9}{n} mV \quad (10)$$

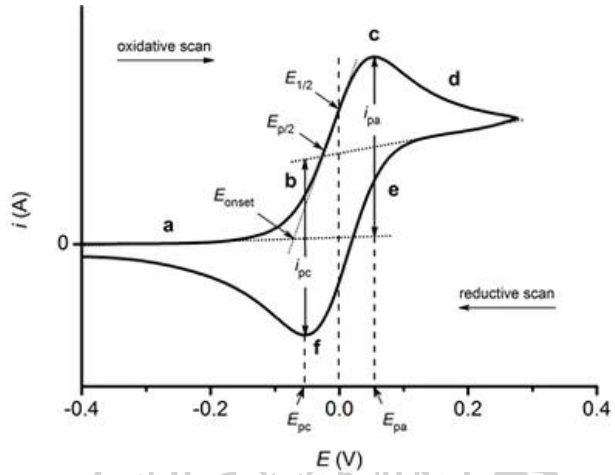

Figure 9 General cyclic voltammogram for a reversible redox reaction [46].

2.3.3.2 Pulse voltammetry

Pulse voltammetry includes techniques such as differential pulse voltammetry (DPV) and square wave voltammetry (SWV). These methods involve applying discrete pulses of potential to the working electrode, and the resulting current is measured.

2.3.3.2.1 Differential pulse voltammetry (DPV)

Differential Pulse Voltammetry (DPV) is an electrochemical measurement technique derived from linear sweep voltammetry or staircase voltammetry. In DPV, a sequence of regular voltage pulses is applied on top of the potential linear sweep or staircase. The current is measured right before each potential change, and the difference in current is plotted as a function of potential. This method helps mitigate the impact of the charging current by sampling the current just before the potential is altered. These measurements are beneficial for investigating the redox properties of extremely low concentrations of chemicals, which is the ability to minimize the impact of charging current, leading to high

sensitivity, and the extraction of only faradaic current, enabling more precise analysis of electrode reactions.

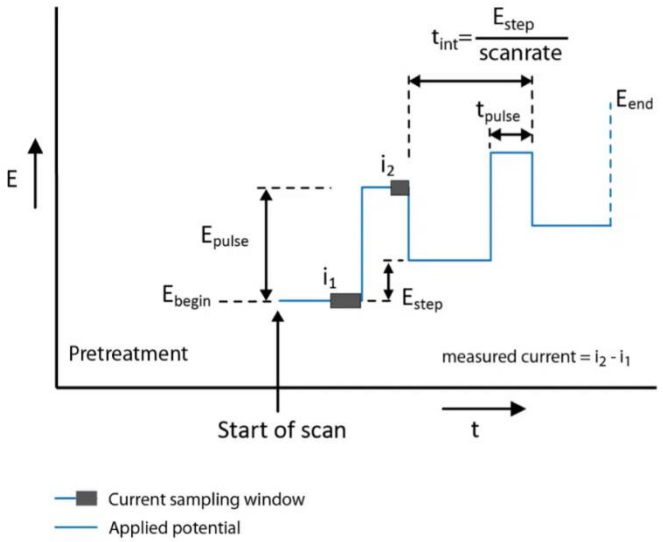

Figure 10 Waveform and measurement scheme of DPV [47].

2.3.4 Working Electrode (WE)

2.3.4.1 Screen printed-carbon electrode (SPCE)

Screen printing technology is employed for the fabrication of biosensors and chemical sensors, replacing the use of large-scale electrodes. Its numerous advantages, such as miniaturization, versatility, and cost-effectiveness, make it highly appealing. Many laboratories opt for screen printing for in-house sensor production. SPCE serves as an alternative material, replacing traditional electrodes and utilizing an economical substrate like ceramic, plastic sheet, or paper. SPCEs have gained success as electrochemical sensors due to their simple production process and swift responses. An additional advantage of SPCE is its single-use nature, eliminating concerns about surface fouling often associated with conventional electrodes. Despite these benefits, electrode modification is occasionally necessary to enhance SPCE performance toward specific target analytes [48, 49].

2.3.4.2 Modifier: Cellulose acetate

Cellulose acetate (CA) refers to an insoluble cellulose derivative, normally cellulose diacetate as shown in Figure 11. This material is synthesized by esterifying hydroxyl groups with acetic acids in cellulose material derived, regarded as a biodegradable and non-toxic material [50]. As a biological membrane, it is used as the modifier for various sensing applications due to its properties like good biocompatibility, stability, inexpensiveness, and environmental friendliness. [51, 52].

Recently, Cellulose acetate has been applied in many electrochemical sensing to determine the number of many substances such as glucose [53], dopamine [54], troponin [55, 56], ochratoxin A [57], catecholamines [58]. Few researchers applied CA to modify the surface of the electrochemical transducer for nitrite sensing as follows.

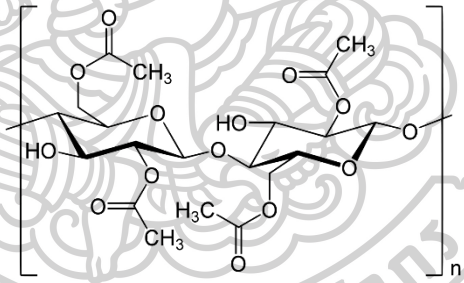

Figure 11 Structural formula of cellulose acetate.

In 2001, Antonella Curulli and her co-workers developed electropolymerized film, cellulose acetate on platinum electrode, for amperometric detection of nitrates and nitrites in water samples by flow injection and batch analysis. Cellulose is applied as a permeable membrane which prevents interference effects at the high applied oxidation potential of nitrite [59].

To achieve cost-effectiveness, small sample volume requirement, disposability, portability, and low detection limit for electrochemical detection of

nitrite, cellulose acetate-modified screen-printed carbon electrodes (CA/SPCE) have been developed as a quantitative analysis part of nitrite in this work.

2.4 Literature reviews

2.4.1 Colorimetric detection of NO_2^-

2.4.1.1 Griess Assay

In 1879, The Griess reaction was primarily reported by Peter Griess as a conventional method for nitrite determination, based on the two sequential chemical reactions in Figure 12. Initially, in the Griess diazotization reaction, sulfanilamide reacts with nitrite form diazonium salt, followed by a reaction with *N*-(1-naphthyl)ethylenediamine (NED) in an azo coupling reaction forming a pink-red azo dye [60].

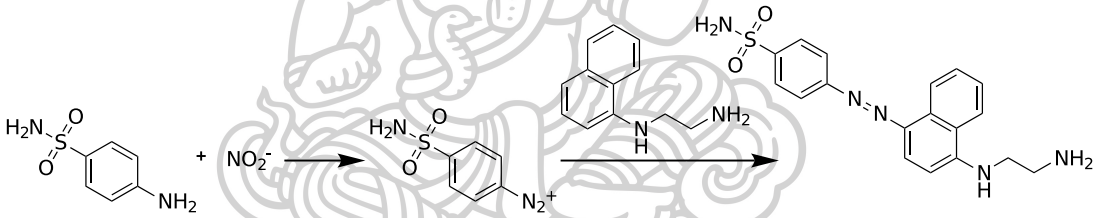

Figure 12 Griess reaction.

To reduce operation time, waste, reagent, and sample volume requirement, the Griess method has been applied to various microfluidic analytical devices in recent years as shown in Table 1.

Table 1 Griess reagent modified on microfluidic devices for nitrite sensing.

Year	Platform	Detection limit	Linear working range	Sample	Reference
2014	Thread-based analytical devices (μ-TAD)	100 μM	0 – 1000 μM	aqueous solution	[61]
2019	Cotton ball-based device	6.56 μM	0-300 μM	artificial saliva	[62]
2015	Microfluidic cloth-based analytical device (μ-CAD)	30 μM	0-500 μM	urine	[63]
2014	Microfluidic paper-based devices (μ-PAD)	1.0 μM	10-150 μM	Synthetic and tap water	[64]
2014	Microfluidic paper-based devices (μ-PAD)	10 μM	10-1000 μM	saliva	[65]
2020	Microfluidic paper-based devices (μ-PAD)	0.40 mg L^{-1} (5.8 μM)	0.40-20.00 mg L^{-1} (5.8-290 μM)	-	[66]
2020	Microfluidic paper-based devices (μ-PAD)	0.1 mg L^{-1} (1.4 μM)	0.5-40 mg L^{-1} (1.4-11.2 μM)	vegetables and processed meats	[67]

Several modified Griess assays have been developed based on the basic concept to enhance the safety, cost-effectiveness, and interference compatibility of reagents. Figure 13 presents the initial principle of the Griess assay. For instance, nitroaniline, sulphanilic acid, and *p*-aminoacetophenone could be utilized as the target amine instead of sulfanilamide. In the same way, 1-amino naphthalene, 1,3-diaminobenzenenaphtholthol, 1naphtholl-4-sulfonate, and phenol were used as coupling agents instead of carcinogenic NED [68].

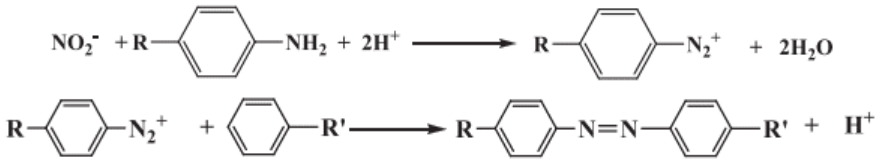

Figure 13 A principle of the Griess assay.

In 2021, Fuangfa Unob and Pitcha Singhaphan developed colorimetric detection of nitrite on a thread-based platform by modified Griess reaction. *p*-aminobenzoyl group, an optional target amine was chemically modified on cellulose thread. Then, cellulose was impregnated with chromotropic acid as a lower toxic coupling agent. In the presence of nitrite, the diazotization and coupling reaction generated an azo-dye color along the length of the functionalized thread. The length of the colored thread depends on nitrite concentration. The linear working range was from 50 to 1000 μM, whereas the lowest concentration that provides color on this thread was 25 μM [69].

Although the Griess reagent is facile and popular, the price is costly and not available in generic. It requires the order via the chemical dealer. Therefore, this work aims to find an alternative reagent to use instead of the Griess reagent for nitrite detection.

2.4.1.2 Potassium permanganate titration

Potassium Permanganate ($KMnO_4$) has a purple color from the metal-to-ligand charge transfer transition. At the endpoint of the titration, acidified $KMno_4$ is possibly reduced from the purple of Mn^{7+} to colorless, brown, and green, corresponding to Mn^{2+}, Mn^{4+}, and Mn^{6+} respectively. [70] Due to an outstanding self-color indicator property of Potassium Permanganate ($KMnO_4$), a strong oxidizing agent is applied for direct and indirect titration to qualitatively determine many substances.

Table 2 Determination of substances by $KMnO_4$ titration

Year	Analyte	Ref.
1924	Sodium thiosulfate	[71]
1935	Oxalate	[72]
1949	Hydrogen peroxide	[73]
1962	Vanadium (V^{4+})	[74]
1970	Nitrite	[75]
1987	Iron (Fe^{2+})	[76]

Permanganometric titration has no need the high-cost instruments, high operation time, and a prominent level of skill. On the contrary, this method settles on benchtop instruments and a large volume of the reagent or sample which produces lots of chemical waste. Due to the benefits and ability of $KMnO_4$, $KMnO_4$ has an attraction to use as the reagent for the development of colorimetric nitrite sensors.

Nowadays, PADs have a lot numerous attention due to their outstanding benefits via capillary action express fluid transport on small and portable paper-based devices without pump requirement, availability of reagent reserving through fiber networks, and high surface area to volume ratio which improves sensitivity for colorimetric approaches [31]. As described earlier, lots of portable microfluidic analytical devices were utilized with Griess reaction on colorimetric detection of nitrite ions for on-site measurements. There are no published microfluidic paper-based analytical devices for nitrite sensing with decolorization reaction of $KMnO_4$.

Then, nitrite-acidified permanganate reaction as shown in the following equation, on microfluidic paper-based analytical devices is invented as a semi-quantitative part of this work.

$$2KMnO_4 + 3H_2SO_4 + 5NaNO_2 \rightarrow 2MnSO_4 + K_2SO_4 + 5NaNO_3 + 3H_2O \quad (11)$$

Nevertheless, the main limitations arise from the disturbance of the color in samples and the relatively low sensitivity of colorimetric detection. To address these challenges effectively, the incorporation of electrochemical detection is particularly

intriguing. Electrochemical detection offers higher sensitivity and the ability to operate precisely even in naturally colored solutions. This is considered a potential solution to the aforementioned issues explored in this dissertation.

2.4.2 Electrochemical detection of NO_2^-

Because of the well-known advantages of electrochemical detection such as ease, low cost, quick response, and good ability for sensing turbid solutions. This method was applied to circumvent the color perturbation of colored samples.

Typically, electrochemical methods involve either oxidation or reduction of nitrite at different solid electrodes. The main problems in the cathodic analysis of nitrite, are interferences from the reduction process of molecular oxygen and nitrate. To avoid this problem, anodic determination of nitrite is preferably performed [77].

There are many types of working electrodes namely, glassy carbon, platinum, diamond, gold, copper, and transition metal oxide electrodes for nitrite sensing. Carbon-based materials such as glassy carbon, carbon paste, graphite, and carbon nanotube are broadly used in electrochemical approaches, due to inexpensiveness, chemical inertness, high specific surface area, low background signal, and wide oxidative potential window [78]. The related study that used various types of modifiers on carbon-based electrodes for the determination of NO_2^- by differential pulse voltammetry (DPV) is summarized in **Table 3**.

Table 3 The modified carbon-based electrodes for the determination of nitrite by DPV.

Year	Electrode	Medium	Linear range	Detection limit	Sample	Ref.
2018	graphene/polypyrrole/chitosan-modified glassy carbon electrode (GCE)	0.1 M NaAc-Hac buffer pH 4.0	0.2 - 1000 μM	0.02 μM	Natural water	[79]
2019	manganese porphyrin/niobium tungstate nanocomposites modified GCE	PBS pH 7.0	0.12- 3.57 mM	0.38 μM	-	[80]
2019	copper ions–crosslinked bovine serum albumin nanoflower networks modified GCE	0.1 M PBS pH 7.4	0.5 - 500 μM	0.1 μM	mineral water	[81]
2020	reduced graphene oxide (rGO)/$MnFe_2O_4$/polyaniline fibrous nanocomposite supported GCE	0.1 M PBS pH 7	0.05 - 1200 μM	0.015 μM	tap water, rainwater, borewell water, and flood water	[82]
2020	tetra L-Methionine cobalt (II) phthalocyanine/ multi-walled carbon nanotubes (MWCNTs)/GCE	PBS pH 7	50 nM - 1.0 μM	35 nM	Beetroot Gravy	[83]
2021	copper ion-based metal-organic gel MWCNTs/GCE	HAc-NaAc buffer pH 4.0	0.3 - 100 μM	86 nM	pickle and sausage	[84]
2022	Gold nanoparticles-polyethyleneimine/SPCE	0.1 M PBS pH 6.5	0.01 - 4.0 μM	2.5 nM	mineral water and olive water	[85]
2022	MnO_2-rGO/GCE	0.1 M PBS pH 7	0.1 - 5.5 μM	0.02 μM	tap water and juice	[86]

2.4.3 Dual detection of nitrite

Attributed to the limitation of colorimetric detection and merits of electrochemical detection. In 2022, Xiagheng Niu, and his co-workers coupled oxidase-mimetic nanozyme and diazotization reaction together for the development of a novel dual-mode double ratiometric electrochemical and colorimetric method for nitrite sensing. The key mechanism of nitrite detection includes two steps of reactions. Firstly, the oxidation of colorless TMB (3,3',5,5'-tetramethylbenzidine), a low toxicity chromogenic substrate is catalyzed by carbon-supported Mn_3O_4 nanocomposite, forming a blue TMBox which displays maximum absorbance at 652 nm. Then, nitrite in the sample solution reacts with TMBox in the diazotization process, generating a visible signal of diazotized TMBox at 445 nm but reducing a signal assigned to TMBox at 652 nm. On the other hand, the anodic signal of TMB on the bare screen-printed carbon electrode (SPCE) decreases while a new anodic signal refers to the oxidation process of nitrite. Thus, these overturned changes of both electrical and optical signals are feasible for dual-mode double-ratiometric analysis of nitrite with detection limits of 1.7 and 0.4 μM respectively [87].

However, their work is not practical to prepare sample solutions for application on two conventional laboratory instruments at the same time. It's preferable to choose only one method to improve sample throughput.

As mentioned above, to reach out practical portable sensor, a single device with dual electrochemical and colorimetric detection for nitrite sensing is fabricated in this work for both non-laboratory skill users and laboratory staff. The simple decolorization of $KMnO_4$ in the presence of nitrite has been used to decrease the cost of reagent and is generally available on the market. In the case of the sample with color or low concentration of nitrite in which the colorimetry could not be performed, the electrochemical technique using the CA/SPCE could be operated in the same device. The proposed sensor with colorimetric and electrochemical detection on a single device offers a simple, cost-effective, and practical tool for the

detection of nitrite contaminated in food and environment with the ability to operate on-site analysis.

CHAPTER III:

EXPERIMENTAL

3.1 Chemicals and Materials

Table 4 List of chemicals and materials.

Chemicals	Chemical formula	Molecular weight	Supplier	Grade
Sodium acetate	$CH_3COONa.3H_2O$	82.03	Merck	ACS reagent
Acetic acid	CH_3COOH	60.05	-	-
Hydrochloric acid	HCl	36.46	-	-
Potassium dihydrogen phosphate	KH_2PO_4	136.09	Merck	ISO
Disodium hydrogen phosphate	Na_2HPO_4	268.07	Merck	ACS reagent
Phosphoric acid	H_3PO_4	97.99	-	-
Sodium sulfate	Na_2SO_4	142.04	-	-
Sulfuric acid	H_2SO_4	98.08	-	-
Sodium hydroxide	NaOH	40.00	RCI Labscan	Reagent grade

Chemicals	Chemical formula	Molecular weight	Supplier	Grade
Lithium perchlorate	$LiClO_4$	106.40	Fluka	ACS reagent
Potassium chloride	KCl	74.56	-	-
Sodium nitrite	$NaNO_2$	39.17	Alfa Aesar	ACS reagent
Potassium ferricyanide	$K_3[Fe(CN)_6]$	329.24	Sigma Aldrich	-
Potassium nitrate	KNO_3	101.10	Merck	ISO
Sodium nitrate	$NaNO_3$	84.99	Ajax fine chem	Analytical reagent
Sodium chloride	NaCl	58.44	-	-
Sodium carbonate	Na_2CO_3	105.10	-	-
Filter paper grade 1	$(C_6H_{10}O_5)n$	162.14	Cytiva	-
Paraffin wax	C_nH_{2n+2} ; n= 22 - 27	300 - 550	-	Food grade
Paraffin oil	C_nH_{2n+2} ; n= 22 - 27	300 - 550	-	-

3.2 Instruments and equipment

Table 5 List of instruments and equipment

Instruments and equipment	Supplier
Potentiostat Sensit BT	Palmsens, Netherlands
Screen-printed template block	Chaiyaboon Co. Ltd., Thailand
pH meter	Mettler Toledo, Switzerland
4-digit analytical balance	Mettler Toledo, Switzerland
Field emission-Scanning Electron Microscope (FESEM)	TESCAN ORSAY HOLDING, Czech Republic
UV-Vis spectrophotometer	Agilent Technologies, USA
Attenuated Total Reflectance (ATR)	PerkinElmer, USA
Hot plate stirrer	IKA Works Co. Ltd, Thailand
Filter paper No.1	Whatman, England
Micropipettes and tips	Labnet International Inc., USA
Light studio box	Puluz, China
Smartphone camera	Apple Inc., USA
Circle hole punches paper diameter 1.3 cm.	EK Success, USA
Milli Q water system (R ≥ 18.2 MΩ cm)	Millipore, USA

3.3 Design and Fabrication

The design of a portable nitrite sensor consists of 2 sheets, an electrode pad, and a colorimetric pad. The configurations of the electrode and colorimetric pads were designed using Adobe Illustrator software (Adobe System, Inc.) as shown in Figure 14.

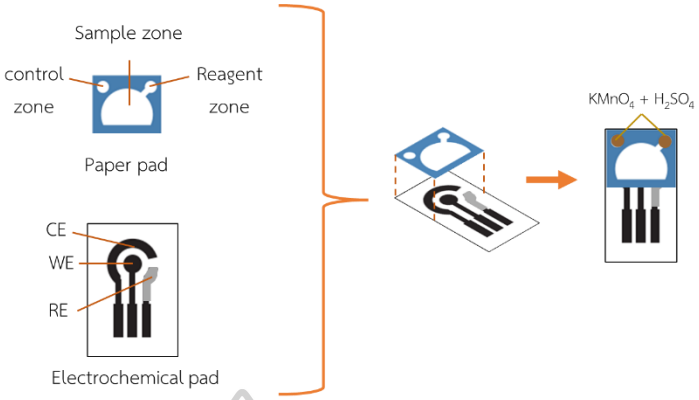

Figure 14 Fabrication of a portable nitrite sensor using the colorimetric and electrochemical dual-mode platform.

For the construction of the colorimetric pad, the designed patterns were created on Whatman No.1 chromatographic paper using a screen-printing technique of a melted mixture of ink which contains solid wax and paraffin oil in the ratio of 1.00 g: 300 µL, followed by the ink curing step at 90 °C for 30 s to allow the penetration of wax into filter paper to define the hydrophobic and hydrophilic areas. The colorimetric pad consists of the control zone (diameter: 4 mm), colorimetric detection zone (diameter: 4 mm), and sample zone (diameter: 8 mm). For the fabrication of the electrode pad, the three-electrode consisting of working, counter, and reference electrodes were constructed onto a PET sheet using the screen-printing technique. The carbon ink was screened on a PET sheet as the working, counter, and conducting pad. Then silver/silver chloride (Ag/AgCl) ink was painted to create the reference electrode. These screen-printed electrodes were cured at 55 °C for 1 h after each layer was printed. To enhance the sensitivity of electrochemical detection, cellulose acetate was weighed and mixed with commercial carbon ink in a mortar using a pestle. This modified ink was subsequently printed onto the working electrode area. After that, the double-sided tape was perforated using a hole puncher (diameter: 1.3 cm) for attachment of the colorimetric paper pad on the electrode sheet.

3.4 Chemical solutions

3.4.1 Electrochemical characterization

To perform electrochemical characterization, the electroactive surface area and charge-transfer resistance (R_{ct}) were assessed in a 2 mM $K_3[Fe(CN)_6]$ in a 0.1 M KCl solution. The electrochemical performance of CA/SPCE was compared with an unmodified SPCE based on analyses of electroactive surface area and R_{ct}. Additionally, the electrochemical behavior and mass transfer process of NO_2^- toward CA/SPCE was investigated in a 0.2 mM NO_2^- solution in 0.1 M Na_2SO_4 at pH 5.0.

3.4.2 The reagent solution for colorimetry

Initially, a 50 mM potassium permanganate ($KMnO_4$) stock solution was freshly prepared by dissolving 0.0316 g of $KMnO_4$ in 2 mL of Milli-Q water. This stock solution was stored in an opaque centrifuge tube. Simultaneously, a 0.1 M sulfuric acid (H_2SO_4) stock solution was independently prepared as a catalyst. These stock solutions were later diluted and combined in specific ratios to achieve the intended concentrations for optimizing reagent proportions.

The optimal reagent concentrations were determined to be 7.5 mM for $KMnO_4$ and 0.7 M for H_2SO_4. This concentration was achieved by mixing 150 µL of the $KMnO_4$ stock solution, 700 µL of the H_2SO_4 stock solution, and 150 µL of water.

3.4.3 Supporting electrolytes

To achieve the best analytical efficiency in both colorimetric and electrochemical detections, various types of supporting electrolytes, including acetate buffer, potassium chloride (KCl), lithium perchlorate ($LiClO_4$), sodium sulfate (Na_2SO_4), and phosphate buffer (PBS) were studied in a fixed pH 4.5.

According to the optimal supporting electrolyte, the influence of the pH of the selected supporting electrolyte was studied. Various pHs in the range of 3.5 to

6.0 (10 mL) were prepared. The solution was adjusted pH by adding H_2SO_4 for lower pH, while NaOH was utilized for upper pH.

3.4.4 Stock standard solution and standard working solution

The 0.1 M of standard stock solutions of NO_2^- were prepared by dissolving in Milli Q water and stored at room temperature until use. Then, the standard stock solution was diluted in 0.1 M Na_2SO_4 pH 5.0 at a desired ratio and used as the standard working solution.

3.4.5 Samples preparation

Vegetable and meat samples, including butterhead, green oak, red oak, salad cos, ham, sausages, and meatballs were purchased from the local market in Nakhon Pathom, Thailand. Vegetables and meat samples were weighed 1 g, crushed, and extracted in 5 mL milli Q water at 80°C and 8000 rpm for 15 min and filtered with nylon membrane to remove remaining suspension particles, the volume of extract solution was adjusted in 5 mL as stock solution Soil was extracted 5 g per 10 mL DI water and filtered with nylon membrane and kept as stock. Tap water was received as a stock solution. All stock solutions were diluted 2-fold with 0.1M Na_2SO_4 pH 5.0 for vegetables, processed food, and soil before measurements.

3.5 Procedure

3.5.1 Electrochemical detection of NO_2^-

3.5.1.1 Electrochemical behavior studies of NO_2^-

Cyclic voltammetry (CV) was used for characterizing the electrochemical behavior of the NO_2^-, and study of the electroactive surface area on the bare SPCE and CA/SPCE. Electrochemical impedance spectroscopy (EIS) was applied to investigate charge-transfer resistance (R_{ct}) for comparison of the unmodified and modified electrodes.

For the qualitative determination of NO_2^-, Differential pulse voltammetry (DPV) was performed in 0.2 mM NO_2^- in 0.1 M Na_2SO_4 with potential applied range 0 to 1.2 V vs Ag/AgCl at a step potential of 50 mV, pulse amplitude 350 mV, and pulse time 15 ms with a scan rate 0.05 Vs^{-1}.

3.5.1.2 Optimization of the electrochemical detection

The effect of supporting electrolyte, pH of supporting electrolyte, the amount of CA, and DPV parameters to the response signal of electrochemical detection of NO_2^-were studied at 0.2 mM NO_2^-. During the optimization, the evaluated parameters were varied, with the constant values of other parameters.

3.5.2 Colorimetric detection

3.5.2.1 Study of the colorimetric reaction of $KMnO_4$ and NO_2^-

The reaction between $KMnO_4$ and NO_2^- is proposed as a key reaction for nitrite detection on colorimetric PADs. A circle design pattern (diameter: 5 mm) of a paper-based device was created by wax-screen printing on filter paper. Then an adhesive tape was placed on the back side of the paper. This paper was utilized for recognizing the decolorization reaction of $KMnO_4$ as shown in Figure 15. The color change was observed by the naked eye.

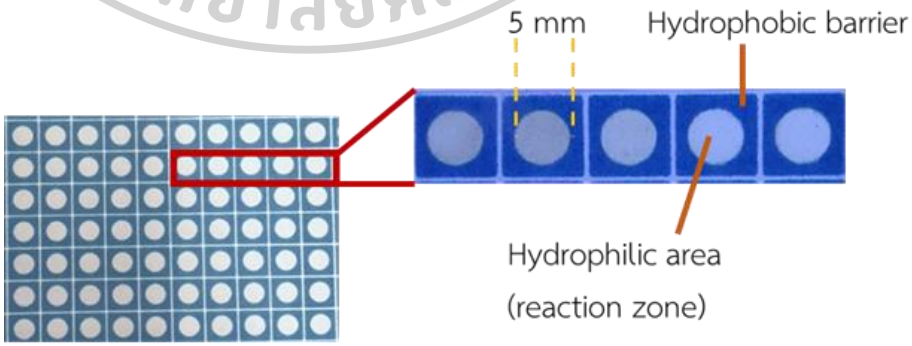

Figure 15 The design pattern for nitrite determination by colorimetric detection.

3.5.2.2 The colorimetric detection using the proposed device

As shown in Figure 14, colorimetric PAD design is composed of three sections that is control zone, reagent zone, and testing zone. To perform colorimetric detection, 1 µL of the acidified $KMnO_4$ mixture was loaded onto a reagent zone and control zone. After waiting for the reagent to dry. Followed by 1 µL of pure supporting electrolytes was loaded to the control zone and 150 µL of the nitrite solution (working standard or sample) was loaded onto a sample zone. After 10 min, the test zone was captured by an iPhone 13 camera under an in-house light-controlled box. The color intensity (red, green, blue, and weighed grayscale intensity) of the testing zone was then analyzed using Image J software using the menu command *Analyze* > *Histogram*. Numerical outcomes were expressed as the Δmean intensity of the RGB color model, determined by measuring the color intensity on the testing zone and subsequently subtracting the value at the measuring point from the blank's signal. Then, the relationship between the Δmean intensity and concentration of NO_2^- was evaluated, leading to qualitative analysis. All measurements were done at least in triplicate.

3.5.2.3 Optimization of the colorimetric detection

The influence of supporting electrolyte, pH of supporting electrolyte, the concentration of $KMnO_4$, the concentration of H_2SO_4, the drying time of reagent, and the reaction time to the response signal of colorimetric detection of NO_2^-were studied at three concentrations, 1, 5, and 10 mM NO_2^-. During the optimization, the evaluated parameters were varied, with the constant values of other parameters.

3.5.3 Analytical performance

3.5.3.1 Calibration curve

Standard solutions and samples were analyzed, and the peak currents were integrated. A calibration curve of standard solutions was examined under optimal conditions and treated with linear least square regression analysis using Microsoft

Excel software for electrochemical detection, while in colorimetric detection, the standard curve was fitted in hyperbolic function, and transformed to a linear relationship. The limit of detection (LOD) and limit of quantification (LOQ) were determined from the $3SD_{blank}$/Slope and 10 SD_{blank}/Slope, respectively, where SD_{blank} is the standard deviation of the response signal, performed in 0.1 M Na_2SO_4 pH 5.0, and Slope is the sensitivity of the method, obtained from the slope of the linearity.

3.5.3.2 Reproducibility

The reproducibility of the proposed sensor was estimated in terms of the relative standard deviation (%RSD) of 6 sheets of electrochemical sensors and colorimetric PADs. The electrochemical and colorimetric detections were performed in 0.3 mM NO_2^- and 0.5 mM NO_2^- in 0.1 M Na_2SO_4 pH 5.0, respectively. The %RSD was calculated from the following formula.

$$\%RSD = \frac{SD}{Mean} x\ 100 \quad (12)$$

Where %RSD =the percentage of the relative standard deviation

SD = the standard deviation of the response signal

Mean = the average of the response signal

3.5.4 Interferences study

Many suspicious species found in foods and agriculture products have been investigated including Li^+, K^+, Ca^{2+}, Fe^{2+}, Fe^{3+}, Ni^{2+}, Cu^{2+}, Zn^{2+}, As^{3+}, NH_4^+, Cl^-, ClO_4^-, HCO_3^-, HPO_4^-, $H_2PO_4^-$, CH_3COO^-, NO_3^-, PO_4^{3-}, borax, glucose, glutamic acid, and urea for selectivity and reported as tolerance ratios. The concentration of NO_2^- at 0.1 mM and 5 mM, is practiced for electrochemical and colorimetric detection respectively. The tolerance limit was defined as the interferent that yielded a relative error less than or equal to 5% when compared to the recorded response of standard concentrations of NO_2^-.

3.5.5 Real samples analysis

For dual-mode detection of nitrite, a part of colorimetric detection, 1 µL of coloring agent containing 7.5 mM $KMnO_4$ and 0.7 M H_2SO_4 was spotted in the control zone and colorimetric detection zone and kept drying for 30 mins, followed by a drop of 150 µL of sample solution. After reaction for 10 mins, the photographs were captured using a smartphone in a light-controlled box. For semi-quantitative interpretation, the obtained photographs were imported and analyzed using the ImageJ program. For the electrochemical process, DPV has applied voltage in the range from 0.0 to 1.2 V vs Ag/AgCl under optimal conditions.

3.5.6 Griess Assay for method validation

2.0000 g of weighed commercial Griess reagent powder was dissolved and adjusted in 50 mL in Milli Q water. The solution was mixed by inversion for 5 mins. The sample solutions were prepared in six concentrations within the working range: 10 - 60 µM NO_2^-. After that, 100 µL of Griess Reagent and 100 µL sample solution were mixed for 15 mins, and then record the absorbance at 540 nm.

CHAPTER IV:

RESULTS AND DISCUSSION

4.1 Electrochemical detection

4.1.1 Morphology characterization

Cellulose acetate (CA) was mixed with carbon ink to modify the electrode surface by screen-printing. The surface morphology of bare SPCE and CA/SPCE was studied using a scanning electron microscope (SEM) in 50.0 kX magnitudes as shown in Figure 16, respectively.

Considering the bare SPCE (Figure 16 (a)), the rough surface was observed due to the carbon ink composition. On the other hand, the surface of the CA/SPCE electrode (Figure 16 (b)) is slightly denser in the modification layer because the porous fiber structure of CA [88-90] has entered into the spaces of the surface of the carbon.

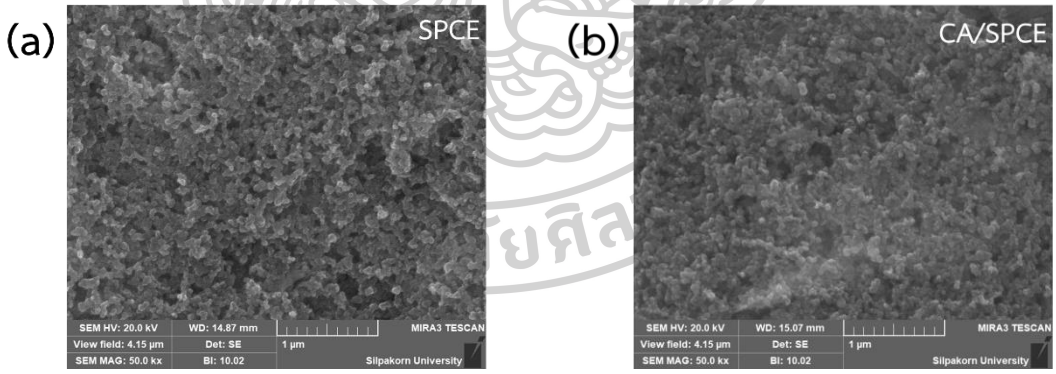

Figure 16 SEM images of bare SPCE (a) and CA/SPCE (b).

4.1.2 Structural Characterization.

To confirm the existence of CA after modification, the infrared (IR) spectroscopy of thin electrodes was operated on an attenuated total reflection (ATR) crystal for

identifying functional groups on bare SPCE and CA/SPCE. The IR source was applied in the wave number range of 4000 to 500 cm^{-1}.

The IR spectrum of CA/SPCE, shown in Figure 17, exhibits some characteristic functional groups of cellulose acetate. The bands at 1728, 1370, 1239, 1019, and 899 cm^{-1} correspond to the stretching vibration modes of C=O of the ester group, C–O asymmetric stretching of the carboxylate group, C–H symmetric bending of the methyl group in the acetate group (–O(C=O)–CH_3), C–O–C asymmetric stretching of ether group in the pyranose ring, and C–H out of plane deformation respectively [91, 92]. The absorption peak at 2885 cm^{-1} is attributed to the methyl group (-CH_3). The broad peak at 3350 cm^{-1} was referred to stretching of the hydroxyl groups (-OH) on intermolecular hydrogen bonds. While the absorption peak is not observed in the spectrum of bare SPCE [93], as predicted. The findings confirm the presence of CA on the surface after modification.

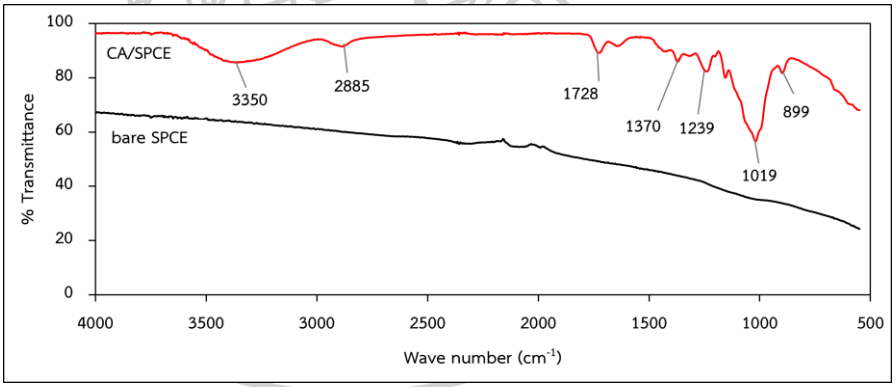

Figure 17 The IR spectra of bare SPCE (black line) and CA/SPCE (red line).

4.1.3 Electrochemical Characterization of CA modified and bare SPCE.

The electrochemical characteristics of the electrodes were evaluated by CV with 2 mM $K_3[Fe(CN)_6]$ solution in 0.1 M KCl with the potential range from -0.4 to 0.6 V vs Ag/AgCl. The comparison of cyclic voltammograms between the bare and CA/SPCE exhibits a reversible process and higher peak current when the CA/SPCE is used, as shown in Figure 18.

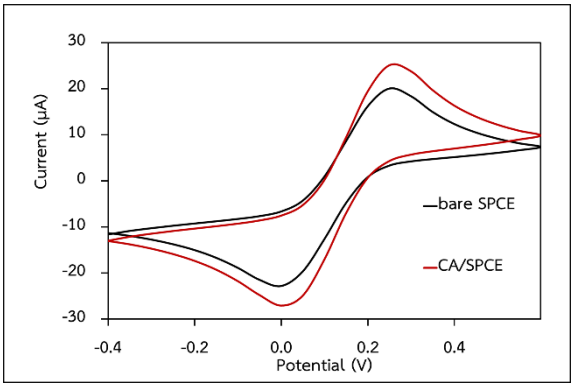

Figure 18 The comparison of CVs performed on SPCE (black line), and CA/SPCE (red line), at 0.05 V s^{-1} using 2 mM $K_3[Fe(CN)_6]$ in 0.1 M KCl.

To prove the performance of CA/SPCE, the electrochemical characteristics exhibited at different scan rates are displayed in Figure 19. In the reversible process, the Randles-Sevcik equation (equation 12) is employed for calculating the electroactive surface area.

$$i_p/v^{1/2} = (2.69 \times 10^5)n^{3/2}ACD^{1/2} \quad (12)$$

where $i_p/v^{1/2}$ is the obtained slope of the relationship between the peak current and square root of the scan rate. n is the number of electrons. A is electrode area (cm^2). C is concentration (2x 10^{-6} mol cm^{-3}). D is diffusion coefficient (7.6 x 10^{-6} cm^2 s^{-1}). The calculated electroactive surface area of bare and CA/SPCE are 0.060 and 0.066 cm^2 respectively. Thus, the electroactive surface from the CA/SPCE is 1.1 higher than the obtained from SPCE.

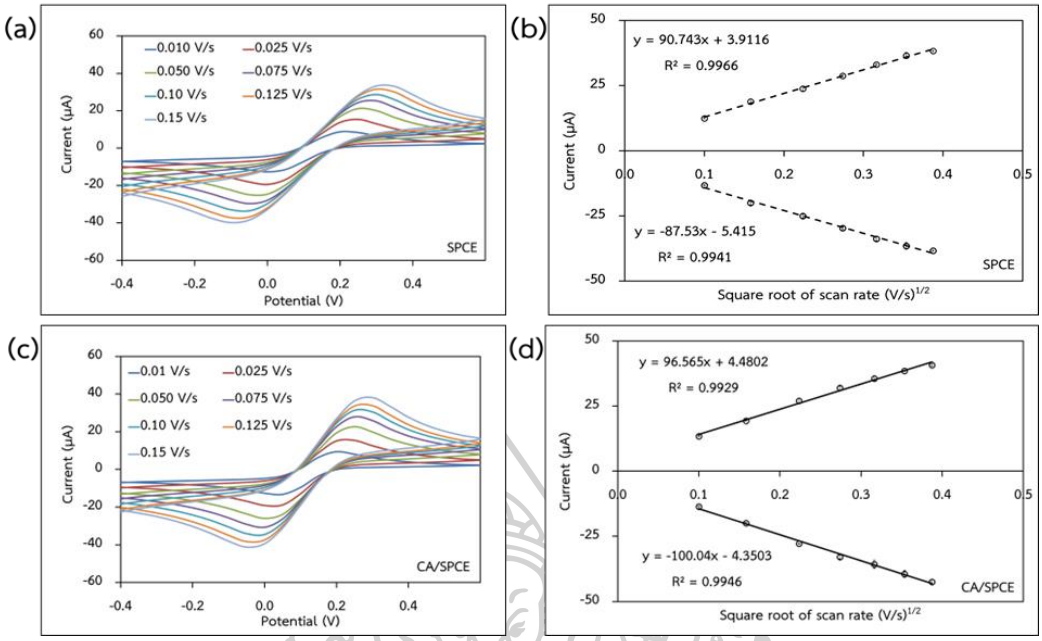

Figure 19 Cyclic voltammograms of SPCE (a), CA /SPCE (c) in 2 mM $K_3[Fe(CN)_6]$ in 0.1 M KCl at scan rates of 0.01, 0.025, 0.050, 0.075, 0.10, 0.125, 0.15 V s^{-1}. In addition, the relationship between the peak current and the square root of the scan rate of SPCE (b), CA /SPCE (d).

Additionally, the comparison of charge-transfer resistance (R_{ct}) on bare SPCE and the CA /SPCE was investigated by electrochemical impedance spectroscopy (EIS) in 2 mM $K_3[Fe(CN)_6]$ in 0.1 M KCl. The electrochemical impedance spectroscopy (EIS) data with Nyquist plots are exhibited in Figure 20. The Nyquist plots indicated a semicircle and a straight line with a 45.0° angle, which represented the charge transfer resistance (R_{ct}) as expected. The charge-transfer resistance in bare SPCE and CA /SPCE were 1715 **Ω** and 1205 **Ω**, respectively. It indicates that the appearance of CA provides better electron transfer.

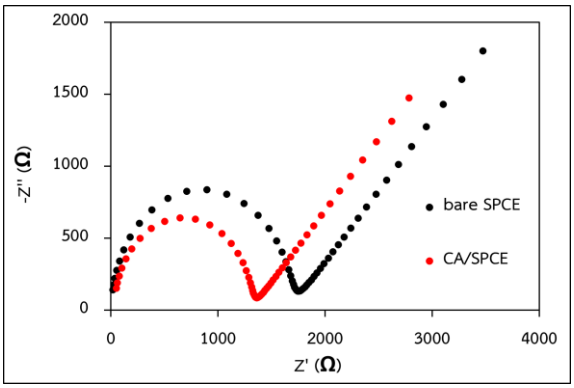

Figure 20 The Nyquist plots of bare and CA/SPCE.

4.1.4 Electrochemical behavior of NO_2^-

CV was used to study the electrochemical behavior of NO_2^- on the bare SPCE and CA/SPCE, as shown in Figure 21. A cyclic voltammogram of 0.2 mM NO_2^- in Na_2SO_4 pH 5.0 with scan rates 0.05 Vs^{-1}. was obtained in the potential range from 0 V to 1.2 V vs Ag/AgCl. From the CV results, the well-defined oxidation peaks of bare SPCE were clearly observed at + 0.70 V vs Ag/AgCl, while the peak current of CA/SPCE was observed at + 0.749 V vs Ag/AgCl. This refers to the oxidation of NO_2^- as shown in equation **2**. In comparison to the results obtained from the SPCE. The anodic peak current on CA/SPCE is found to be obviously higher. The results imply that the use of CA can improve the sensitivity of the sensor.

$$NO_2^- + H_2O \longrightarrow NO_3^- + 2H^+ + 2e^- \quad (2)$$

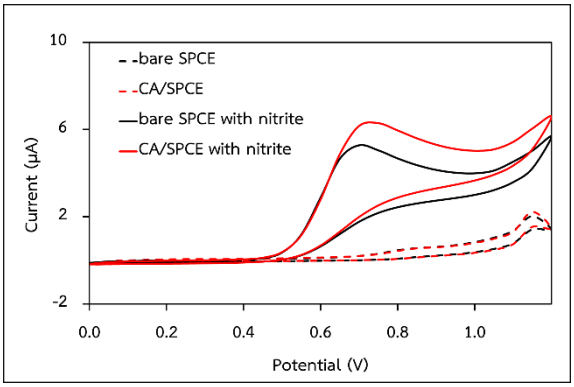

Figure 21 CV curves (of the SPCE (black), and CA/SPCE (red) using 0.2 mM NO_2^- in Na_2SO_4 pH 5.0 with a scan rate of 0.05 Vs^{-1}.

For the quantitative analysis of NO_2^-, DPV was operated on the proposed sensor, as shown in Figure 22. The differential pulse voltammogram of 0.2 mM NO_2^- was investigated in the potential range from 0 V to 1.2 V vs Ag/AgCl. From the DPV results, the oxidation peaks on the bare SPCE and CA/SPCE were clearly observed at + 0.55 V vs Ag/AgCl, related to the nitrite oxidation process. The anodic peak current of the nitrite on CA/SPCE is found 1.3 times higher, compared to the obtained anodic peak current on the bare SPCE which is consistent with the calculated electroactive surface area and the observed R_{ct}.

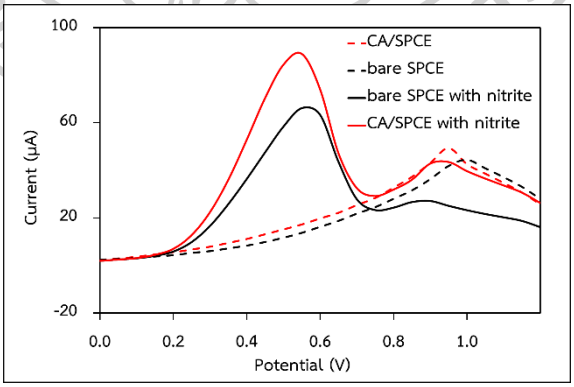

Figure 22 DPV curves of the SPCE (black), and CA/SPCE (red) using 0.2 mM NO_2^- in Na_2SO_4 pH 5.0 with a scan rate of 0.05 Vs^{-1}.

CV was performed at different scan rates to evaluate the mass transfer of the analytes toward the electrode surface. As shown in Figure 22, the anodic current

increased with an increasing scan rate. The better coefficient of the relationship between the square root of the scan rate and the peak current of NO_2^-, compared to the relationship between the scan rate and the peak current was observed indicating that the mass transport of NO_2^- to the CA/SPCE surface was controlled by a diffusion process.

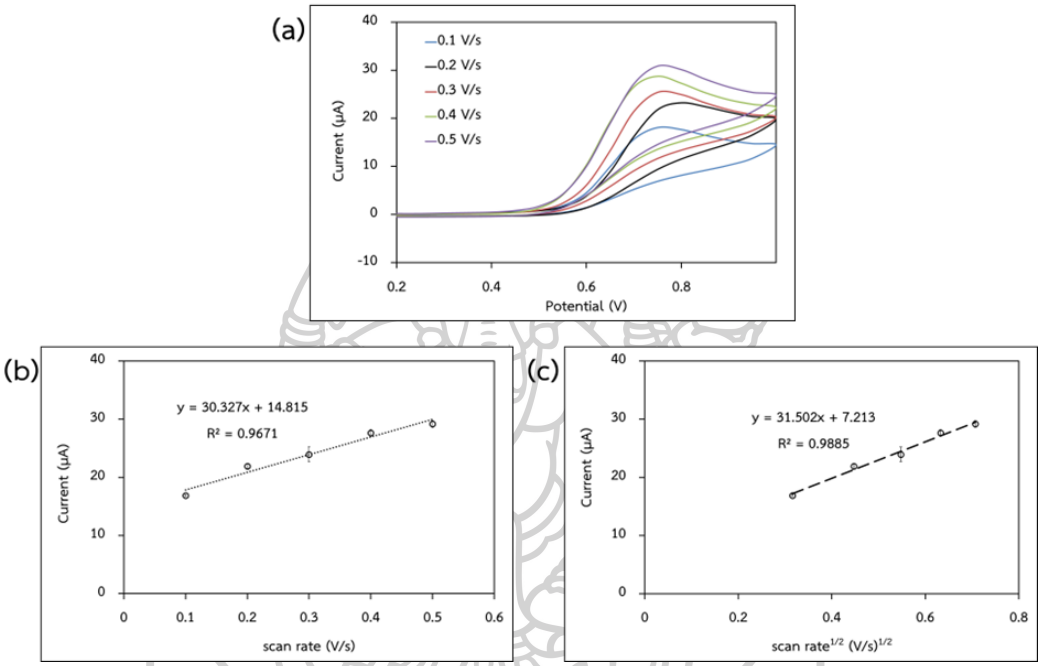

Figure 23 CV curves of different scan rates (a) using 0.2 mM NO_2^- in Na_2SO_4 pH 5.0 the relationship between obtained anodic current and scan rates (b) and the relationship between obtained anodic current and square root of scan rates (c).

4.1.5 Optimization of experiment parameters

4.1.5.1 Supporting electrolytes.

Various kinds of supporting electrolytes such as acetate buffer, potassium chloride (KCl), lithium perchlorate ($LiClO_4$), sodium sulfate (Na_2SO_4), and phosphate buffer (PBS) were studied to reach the best sensitivity of electrochemical detection of nitrite by DPV. All supporting electrolytes had fixed at a pH of 4.5.

As a result, the acetate buffer demonstrated an excellent anodic current signal for NO_2^-. However, a small anodic peak at + 0.6 V appeared in the blank,

leading to a low signal-to-noise ratio. As a result, sodium sulfate (Na_2SO_4) and phosphate buffer (PBS) were chosen for comparison in the optimization to manipulate the optimal conditions for colorimetric detection.

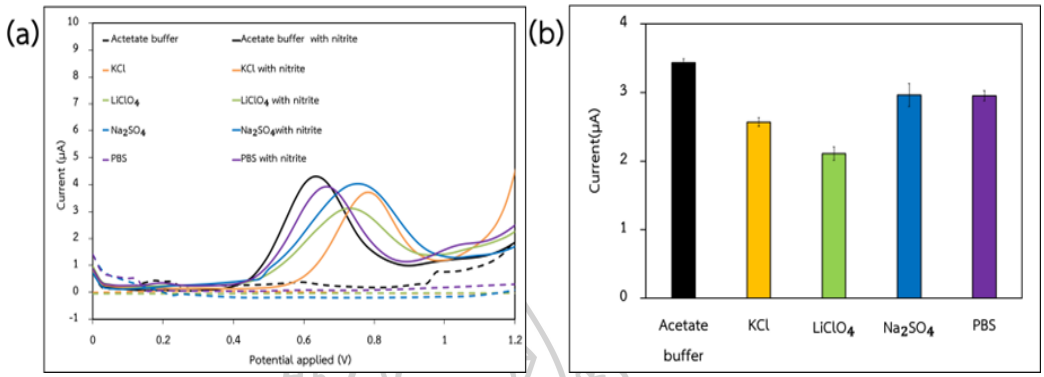

Figure 24 CV curves of various supporting electrolytes (a) and the related measured value (b) of acetate buffer (black), KCl (yellow), $LiClO_4$ (green), and PBS (purple).

4.1.5.2 pH of supporting electrolytes

Because pH directly affects the amount of H^+ or H_3O^+ in the system. The initial pH of 0.1 M Na_2SO_4 supporting electrolytes before this experiment is 4.5. To reach the best sensitivity of electrochemical detection of nitrite, Differential pulse voltammetry (DPV) was operated in 0.2 mM NO_2^- in 0.1 M Na_2SO_4 solution in varied pHs ranging from 3.5 - 6.5.

The optimal pH was 5.0 which displays the highest current. At lower pH, the decrease in an electro-oxidation signal can be ascribed to the instability of the predominant electroactive species HNO_2 (pKa =3.3 at 25 °C) [94]. On the other hand, at pH >5, the formation of oxide layers on the surface of the transducer can be promoted to inhibit the oxidation reaction of nitrite [94].

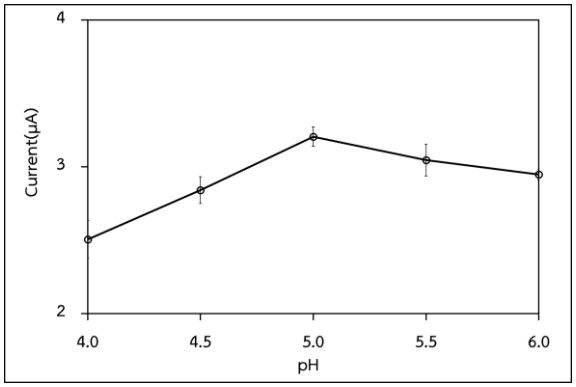

Figure 25 The effect of pH of supporting electrolyte for electrochemical detection.

4.1.5.3 The amount of cellulose acetate (CA)

Cellulose acetate (CA) plays a pivotal role in the oxidation of NO_2^-. The optimization of the amount of CA for the preparation of the CA/SPCE was done by varying the percentage of CA in the carbon ink. The effect of the percentage of CA on the oxidation of NO_2^- was displayed as shown in Figure 26. The oxidation current of nitrite is continuously enhanced with increasing the percentage of CA and maximized at 1.0% (w/v). It corresponds to a characteristic property of CA, a positively charged membrane. Even if its structure is out of basic groups, the direction of the dipole moment of nitrite is opposite to that of the acetyl group. Presumably, a highly polar C=O bond is the most effective part of the structure [95]. Thus, the possibility of analytes towards the transducer surface should be increased. On the other hand, with the further increased amount of this polymer, the signal is decreased because the ability of electron transfer is obstructed by its low conductivity.

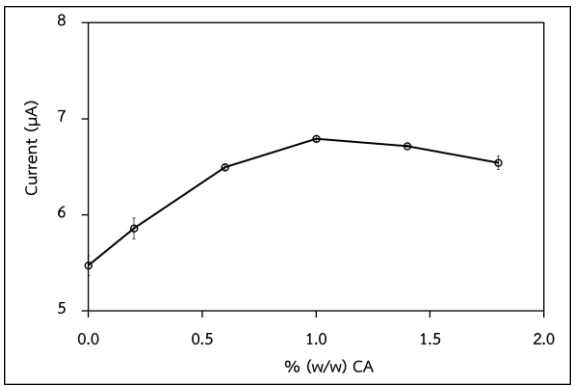

Figure 26 The effect of the amount of cellulose acetate.

4.1.5.4 DPV parameters

DPV was performed in the quantitative analysis of nitrite to record the electrochemical signal and interpret the anodic peak current. The DPV parameters including step potential, pulse amplitude, and pulse time were optimized because these parameters affected the sensitivity for the detection of nitrite. The step potential, pulse amplitude, and pulse time were investigated in the range of 25 - 125 mV, 50 - 400 mV, and 0.1-100 ms, respectively. The studied parameters were kept constant during the optimization. The optimal DPV parameters were found at a step potential of 50 mV, pulse amplitude of 350 mV, and pulse time of 15 ms with a scan rate of 0.05 Vs^{-1}.

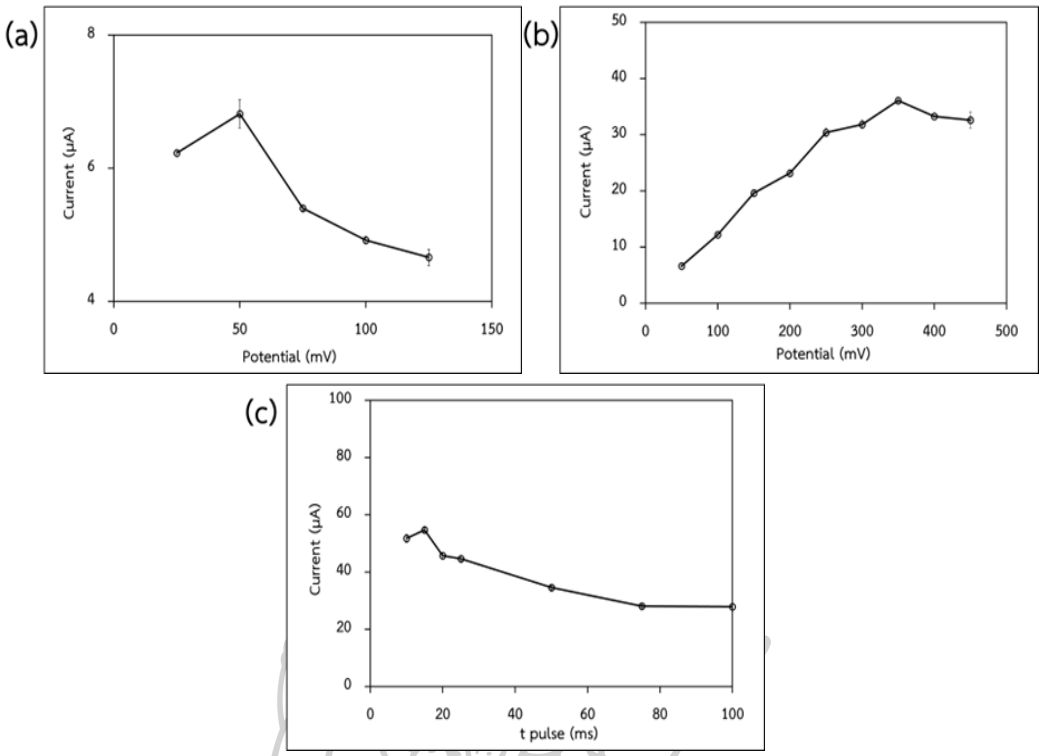

Figure 27 The effect of step potential (a), pulse amplitude (b), and pulse time (c).

4.2 Colorimetric detection

4.2.1 Study the colorimetric reaction of $KMnO_4$ and NO_2^-

In previous work, the mixture of $KMnO_4$ and H_2SO_4 was dropped on a design pattern for colorimetric detection of nitrite. After 1 hour, Different concentrations of nitrite standard were then dropped on the pattern as shown in Figure 30.

As a result, the color of $KMnO_4$ was decolorized by increasing nitrite concentration.

$$2MnO_4^- + 5NO_2^- + 6H^+ \longrightarrow 2Mn^{2+} + 5NO_3^- + 3H_2O \quad \textbf{(3)}$$

Thus, this permanganometry reaction can be successfully applied to the colorimetric detection of nitrite on the paper-based device. Moreover, this $KMnO_4$ reagent system is more cost-effective and more available in general purchasing than the Griess reagent.

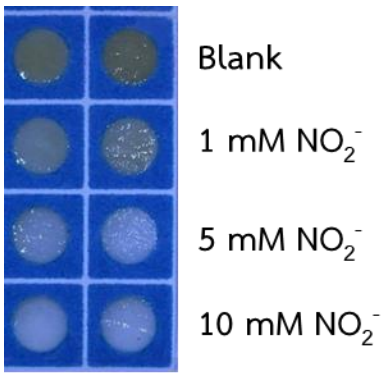

Figure 28 Preliminary results for nitrite determination by colorimetric detection.

To integrate electrochemical and colorimetric platforms in a single device, the colorimetric PADs were designed as shown in Figure 14 and applied in all colorimetric experiments. The sample zone is a semi-circle area for dropping sample solution for dual detection of nitrite, which connects to the testing zone of the colorimetric pad. The control zone was aligned parallel with the testing zone. The control zone is proposed for two purposes. First, it is used as a naked eye-checker of the availability of the colorimetric sensor at that time. Second, it is applied for the subtraction of the surrounding effects on the reagent due to photosensitivity of $KMnO_4$.

4.2.2 Optimization of experiment parameters

4.2.2.1 Supporting electrolytes

Various kinds of supporting electrolytes were studied as same as described in a part of electrochemical detection. All supporting electrolytes were prepared with a fixed pH of 4.5.

As above mentioned in the part of electrochemical detection, to compare different supporting electrolytes between phosphate buffer (PBS) and sodium sulfate (Na_2SO_4), sodium sulfate provides a higher significant response than those obtained from phosphate buffer. In the colorimetric reaction of $KMnO_4$, H_2SO_4 was used to acidify $KMnO_4$. Na_2SO_4 contains SO_4^{2-} ion which proves that this supporting electrolyte

would not interrupt this decolorization system. Thus, 0.1 M Na_2SO_4 is selected as optimal supporting electrolytes.

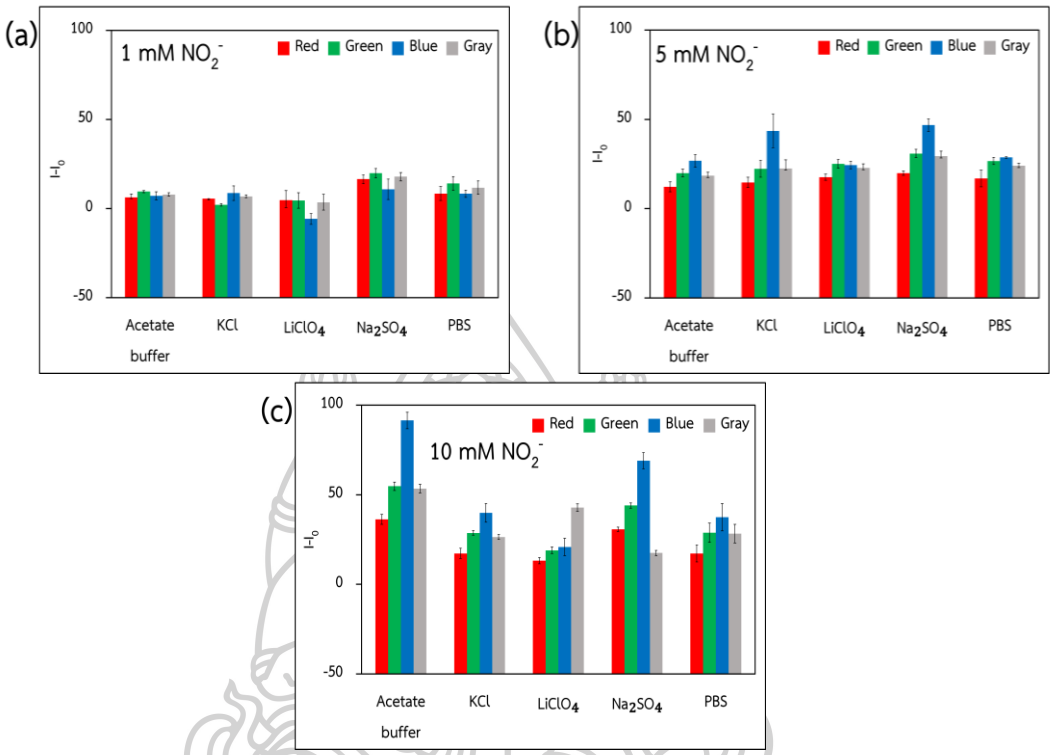

Figure 29 The effect of supporting electrolytes for colorimetric detection at 1 mM (a), 5 mM (b), and 10 mM (c) NO_2^-.

4.2.2.2 The pH of supporting electrolytes.

The initial concentration of the reagent was 10 mM $KMnO_4$ and 0.4 M H_2SO_4 while NO_2^- standard solutions were prepared in 0.1 M Na_2SO_4 pH 4.5. To evaluate the best performance of colorimetric detection, the pH range of 4.0 - 6.5 was studied.

Although there is no significant difference in color sensitivity between pH 5.0 and 5.5 at 5mM NO_2, the highest current is observed at pH 5.0. So pH 5.0 is chosen as an optimal pH of supporting electrolytes due to the stability of nitrite as above mentioned in the electrochemical section [94].

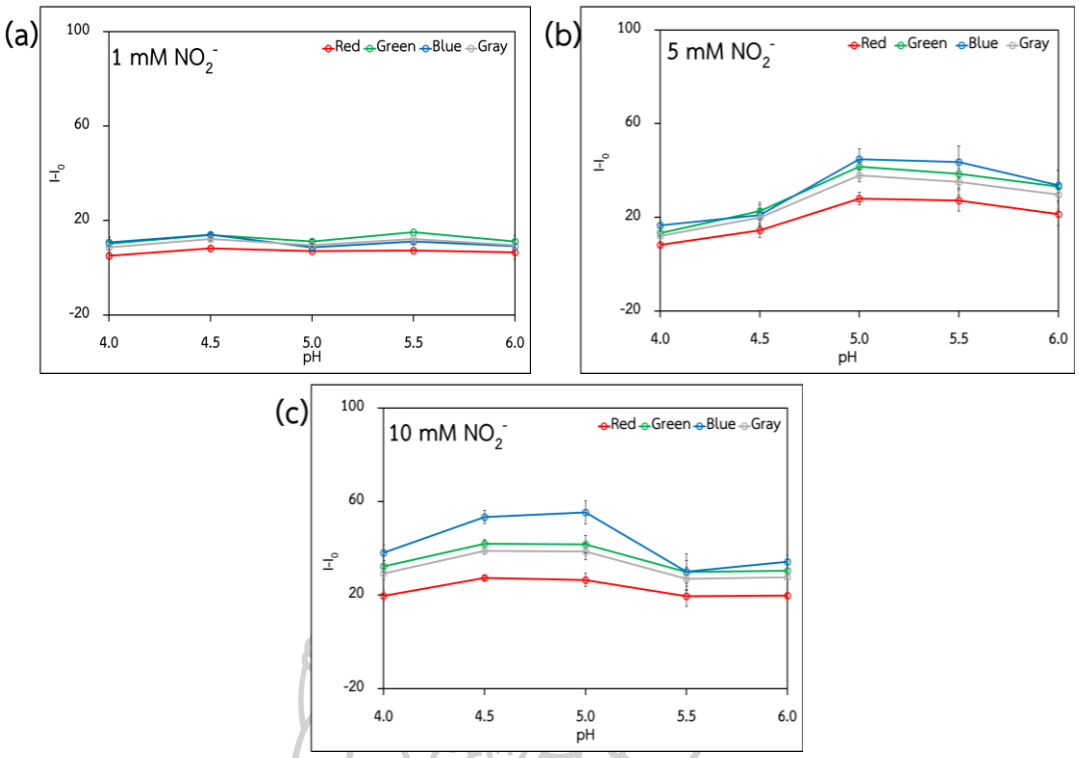

Figure 30 The effect of pH of supporting electrolytes for colorimetric detection at 1 mM (a), 5 mM (b), and 10 mM (c) NO_2^- in 0.1 M Na_2SO_4.

4.2.2.3 The concentration of $KMnO_4$

The initial concentration of the reagent was 10 mM $KMnO_4$ and 0.4 M H_2SO_4 while nitrite standard solutions were prepared in 0.1M Na_2SO_4 pH 5.0. To evaluate the best performance of colorimetric detection, the concentrations of $KMnO_4$ were investigated ranging from 5.0-15.0 mM.

The optimal concentration of oxidizing agent was 7.5 mM $KMnO_4$ which displays the highest efficiency for colorimetric changes at 5 mM and 10 mM of NO_2. A lower concentration of $KMnO_4$ leads to an insufficient oxidizing agent for the decolorization reaction on the high concentration of nitrite. A higher concentration of $KMnO_4$ tends to result in an excessively intense color. Therefore, the concentration of $KMnO_4$ was selected at 7.5 mM.

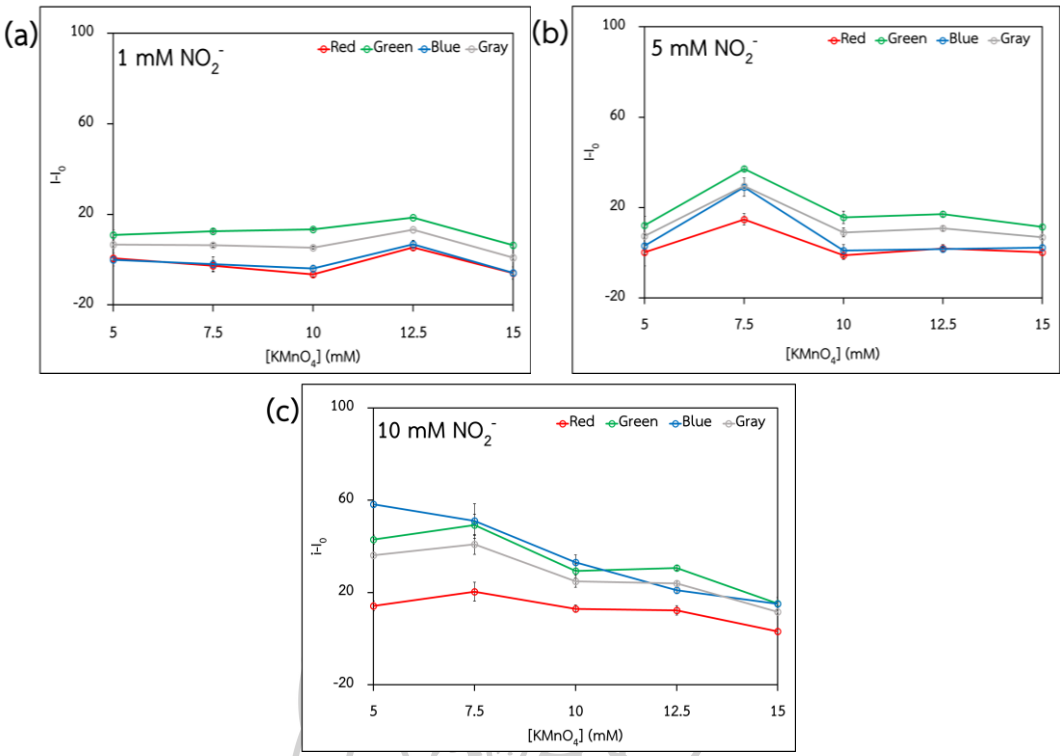

Figure 31 The effect of concentration of $KMnO_4$ for colorimetric detection at 1 mM (a), 5 mM (b), and 10 mM (c) NO_2^- in 0.1 M Na_2SO_4.

4.2.2.4 The concentration of H_2SO_4

The initial concentration of the reagent was 7.5 mM $KMnO_4$ and 0.4 M H_2SO_4 while nitrite standard solutions were prepared in 0.1M Na_2SO_4 pH 5.0. To evaluate the best performance of colorimetric detection, the concentrations of H_2SO_4 were investigated ranging from 0.2 - 0.8 M.

At 1mM NO_2, a higher concentration of acid provides higher intensity and steady intensity around 0.7-0.8 M H_2SO_4. At 5 and 10 mM NO_2, 0.7 M H_2SO_4 displays the highest sensitivity. Lower concentrations of H_2SO_4 provide lower colorimetric sensitivity due to the poor acidic condition for $KMnO_4$ decolorization while too high concentrations of H_2SO_4 might decrease nitrite stability [94]. Then, 0.7 M was chosen as an optimum concentration of H_2SO_4.

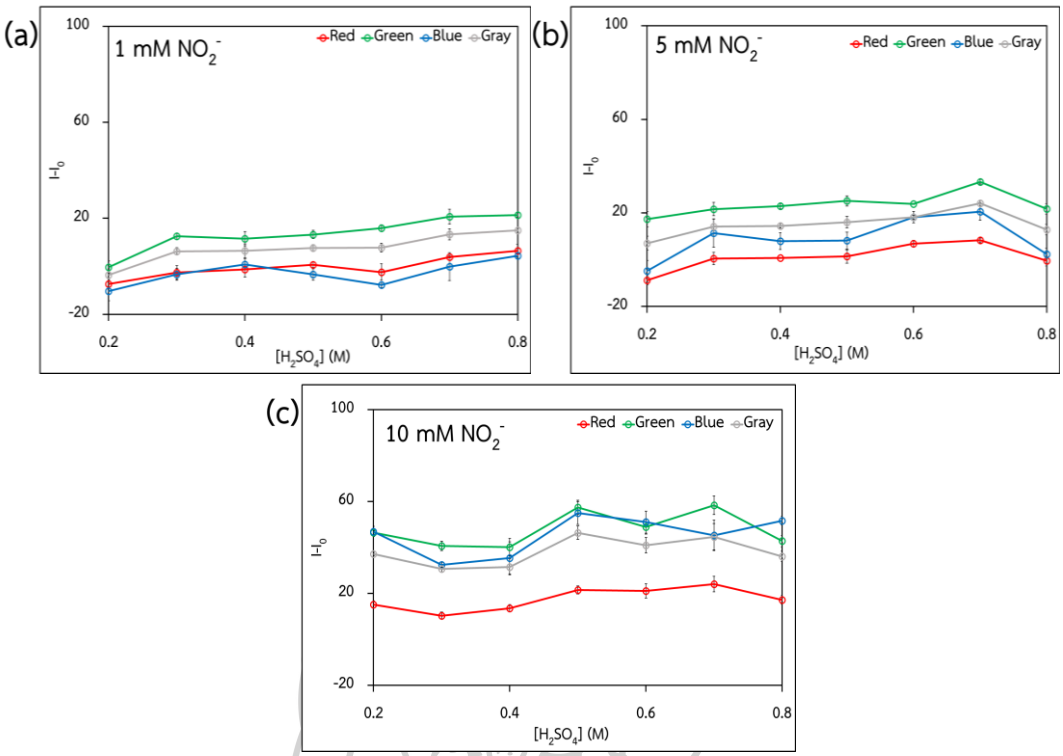

Figure 32 The effect of concentration of H_2SO_4 for colorimetric detection 1 mM (a), 5 mM (b), and 10 mM (c) NO_2^- in 0.1 M Na_2SO_4.

4.2.2.5 The drying time of the reagent

Since using a strong oxidizing agent, the color of $KMnO_4$ can be changed in an acidic solution when it is applied to the paper-based device. To evaluate the best performance of the colorimetric sensor, a reagent drying time was studied in the range of 5-90 min.

Due to a black MnO_2 formation, the reddish-pink reagent mixture slightly turns brown when the drying time increases, and the darkest brown appears at 30 min. However, the brown color is decolored after 30 min from the reduction process in the reagent mixture which also produces a colorless Mn^{2+}. The highest intensity between with and without nitrite, measured by ImageJ results at 30 min, corresponding to the color from the photos and naked-eye observation

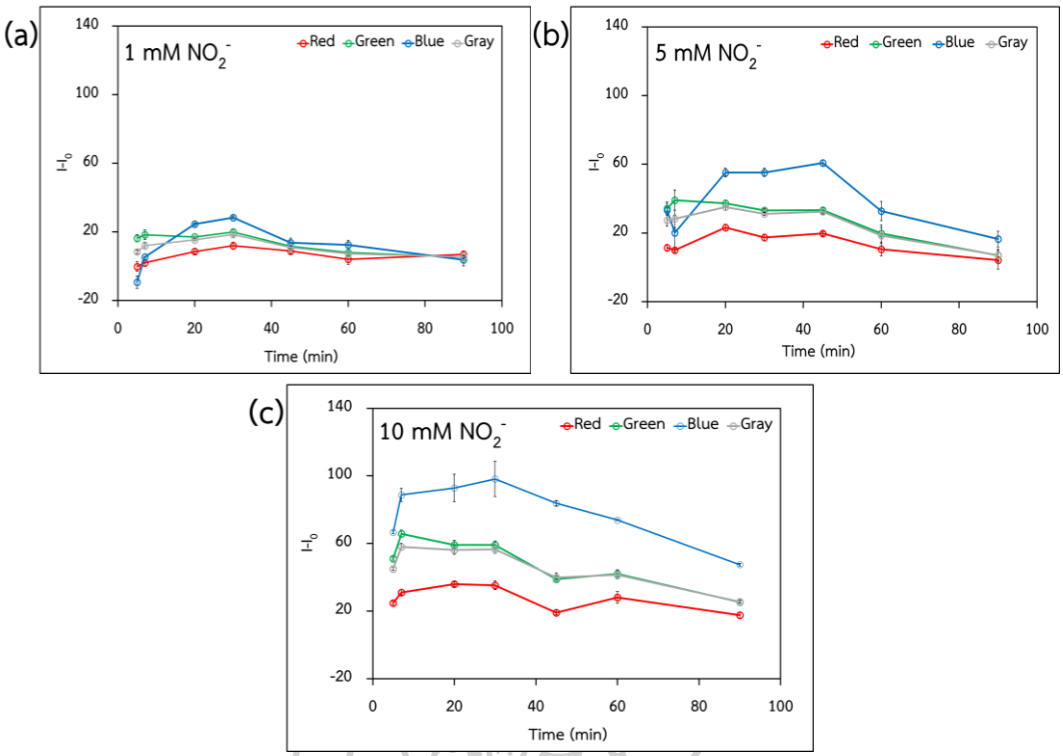

Figure 33 The effects of drying time of reagent for colorimetric detection 1 *mM (a)*, 5 *mM (b)*, *and* 10 mM *(c)* NO_2^- in 0.1 M Na_2SO_4.

4.2.2.6 The reaction time of acidified $KMnO_4$ and NO_2^-

Since decolorization is a time-dependent reaction, the reaction time was investigated in the range of 0-30 min to conquer the highest sensitivity of colorimetric detection.

As a result, the decolorization tends to increase and steady at 5 mins following to kinetics of the reaction. The decrease was found to be over 15 mins due to the over-decolorization of $KMnO_4$ reagent by an acidic medium. Thus, the optimal reaction was set at 5 min.

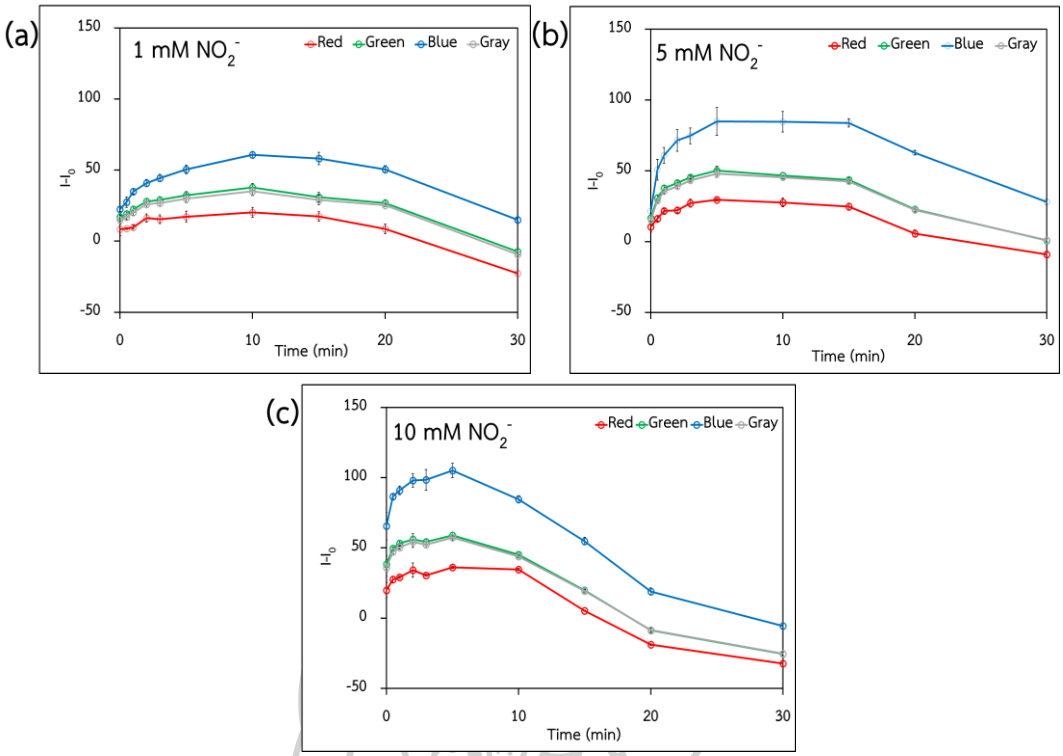

Figure 34 The effect of reaction time for colorimetric detection at 1 mM (a), 5 mM (b), and 10 mM (c) NO_2^- in 0.1 M Na_2SO_4.

4.3 Analytical performances

After studies of all influencing factors, the analytical performance of the developed nitrite sensor has been evaluated. For electrochemical detection, the calibration curve has been constructed between the relationship of the peak current of the related NO_2^- oxidation process and the concentration of NO_2^- in the mM unit.

As shown in Figure 48, the satisfied analytical performance of electrochemical detection was observed. the linearity was observed in the range of 0.05 to 0.6 mM of NO_2^-, with an equation and a correlation coefficient (y =246.7799x -1.8334, R^2= 0.9980). The limit of detection (LOD) has been calculated as 3 × standard deviation (n=6) and divided by slope (3SD/slope), and the limit of quantification (LOQ) has been computed using 10SD/slope. LOD and LOQ of the electrochemical approach were 8.00 and 28.0 µM, respectively. The reproducibility (n=6) was operated using 0.3

mM NO_2^- in 0.1M Na_2SO_4 pH 5.0 is reported in % relative standard deviation (%RSD=3.39%). The stability of electrodes is more than 60 days.

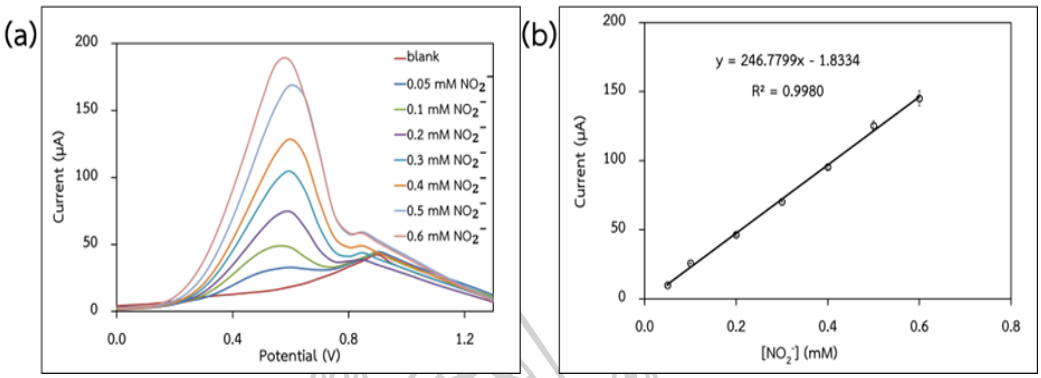

Figure 35 The voltammograms (a) with various concentrations of NO_2^- and the related calibration curve (B) of the electrochemical detection.

In the colorimetric detection, the calibration curve has been performed by illustrating the relationship between the intensities of the corresponding $KMnO_4^-$ decolorization in the presence of NO_2^- and the logarithm function of the concentration of NO_2^- in the mM unit. The results as shown in Figure 49 and summarized in Table 6. Among the RGB index, the best sensitivity with a good correlation coefficient was observed on the blue channel. The differentiation of the proposed reagent color starts from an observed brown stain of a mixture of purple MnO_4^- and black MnO_2 and subsequently turns to colorless Mn^{2+} in the appearance of NO_2^- was observed. The lower absorbance around 525 nm and 230 nm on absorption spectra of increasing NO_2^- concentration were reported in our previous work [96]. Aligned to the opponent process theory [97], the indicated color which is opposite to the complex color of the reaction, exhibits notably on the blue channel. The linear equation by considering on blue channel was obtained in the range of 0.50-10 mM (y = 55.28x +49.75, R^2= 0.9923) and is further used for the analysis of the samples. LOD and LOQ are 0.11 and 0.35 mM, respectively.

The detection limit closely approaches the acceptable daily intake level of NO_2^- in drinking water, as regulated by WHO standards. Hence, the colorimetric aspect of the dual-mode sensing mechanism holds promise for implementation as a NO_2^- screening device in drinking water. A faded color on the testing zone relative to the control zone indicates the detection of an excessive NO_2^- level. Conversely, if the color of the testing zone remains unchanged compared to the control zone, electrochemical detection is employed for precise quantitative analysis.

Table 6 Analytical performance of colorimetric detection of nitrite on the proposed sensor

Color	Red	Green	Blue	Weighed grayscale
Linear range (mM)	1 - 40	0.50 - 40	0.50 - 10	0.50 - 40
equation	y = 22.89x +11.93	y = 26.05x +29.86	y = 55.28x +49.75	y = 26.60x +28.08
R^2	0.9425	0.9889	0.9923	0.9882
LOD (mM)	0.16	0.15	0.11	0.14
LOQ (mM)	0.54	0.49	0.35	0.45
Reproducibility at 5 mM NO_2^- (%RSD, n=6)	2.28	1.81	0.91	1.78

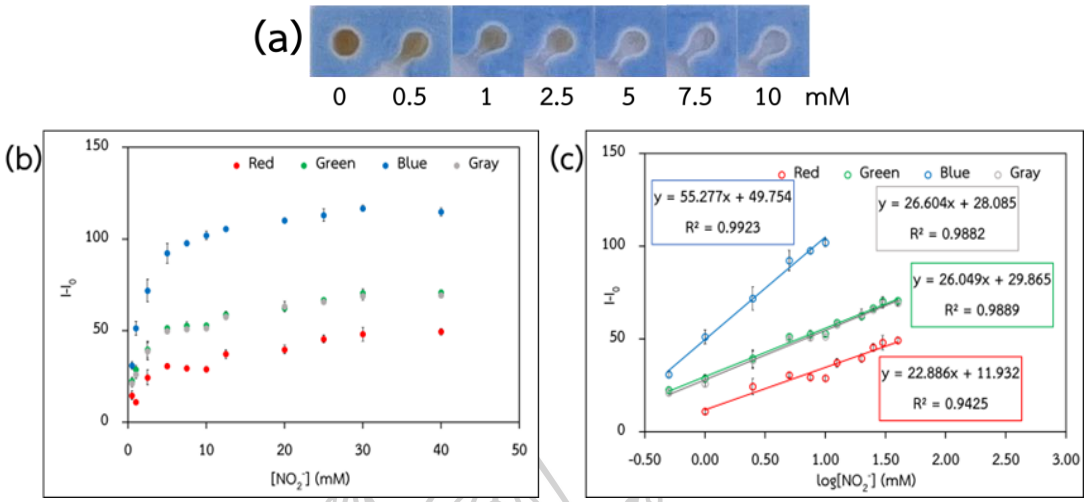

Figure 36 The calibration curve of the colorimetric detection.

4.4 Interference studies

Selectivity is also a significant factor in the accuracy of the proposed determination. Many suspicious species were investigated for selectivity effects and reported as tolerance ratios as summarized in Table 7 and Table 8. The criteria for an acceptable difference level are set within +/- 5% of the average reference value after adding foreign species to the system. The results indicate that the dual-mode sensor has good selectivity for the detection of nitrite.

Table 7 Tolerance ratios of interfering substances in the electrochemical detection of 0.1 mM NO_2^- in 0.1 M Na_2SO_4

Interferences	Tolerance limit
K^+, As^{2+}, Cl^-, HPO_4^-, NO_3^-, $S_2O_3^-$, glucose	1000
Li^+, Ca^{2+}, Zn^{2+}, HCO_3^-, CH_3COO^-, ClO_4^-, urea	100
borax	10
NH_4^+, Cu^{2+}, Fe^{2+}, Fe^{3+}, Ni^{4+}, $H_2PO_4^-$, glutamic acid	5
PO_4^{3-}	1
Mn^{2+}, CO_3^{2-}	-

Table 8 Tolerance ratios of interfering substances in the colorimetric detection of 5 mM NO_2^- in 0.1 M Na_2SO_4

Interferences	Tolerance limit
K^+, NH_4^+, Cl^-, HPO_4^-, NO_3^-	1000
Mg^{2+},SO_4^{2-}	500
Li^+, Zn^{2+}, Mn^{2+}, $H_2PO_4^-$, CH_3COO^-, ClO_4^-, glucose, glutamic acid	200
HPO_4^-	100
PO_4^{3-}	50
Ca^{2+},Cu^{2+}, Ni^{2+}, Fe^{2+}, Fe^{3+},As^{3+}, CO_3^{2-}, borax	5
HCO_3^-	1

4.5 Real sample analysis

The effectiveness of this method was assessed for its applications in the determination of NO_2^- in real samples. All the samples were spiked with 2 sets of the NO_2^- standard concentrations were directly loaded into the proposed sensor to evaluate the matrix effect and concentration of NO_2^-. The first group includes 0.1, 0.2, and 0.3 mM of NO_2^- applied with electrochemical detection. The second group includes 1, 2, and 4 mM of NO_2^- applied with colorimetric detection. The results are shown in Table 9.

The percentage of recovery was calculated from the formula:

$$\%recovery = \left(\frac{C_{std\ spiked} - C_{samples}}{C_{spiked}}\right) x\ 100\ \% \qquad (13)$$

where $C_{std\ spiked}$ is the concentration of spiked standard NO_2^-solution, $C_{samples}$ is the concentration of the sample, and C_{spiked} is the concentration of standard NO_2^-.

To test the practice of the sensor, the determination of NO_2^- using the proposed sensor was compared to the conventional Griess assay. For sample analysis including butterhead, green oak, salad cos, bologna, ham, meatball, tap water, and soil, the paired T–test between the two methods at a 95% confidence level proved that the proposed method was not significantly different from the traditional Griess assay (t_{stat} (-0.041) < $t_{critical}$ (1.673)). The accuracy of the proposed sensor was calculated with respect to the spike concentrations of NO_2^-. The recoveries were found to be 91 to 108%, indicating high accuracy. The high precision of the proposed sensor was observed within the range of 0.10% to 4.7%, derived from 5 replicate measurements at the studied concentrations.

However, when dealing with reddish color samples such as red oak, the presence of a similar shade in the sample's color to that of the reagent color can directly interfere with nitrite determination. This challenge has been effectively addressed through the collaboration of color-independent and highly sensitive methods, such as electrochemical detection. While solely relying on electrochemical techniques poses limitations due to the need for specific skills and equipment, the integration of a straightforward colorimetric method, based on visual color perception and employing a simple $KMnO_4$ reagent, expands accessibility to users and applications.

In scenarios involving the analysis of consumable water, such as tap water, the colorimetric pad can serve as a cutoff device to determine the overdose level of NO_2^- for consumption in accordance with WHO standards.

Moreover, the concentrations of NO_2^- in real samples were calculated. The content of NO_2^- is not observed in all vegetables and soil samples. While in bologna, ham, and meatballs were detected in 59.8, 69.0, and 78.2 mg/kg of each sample, respectively. It also found 4.60 mg/L of NO_2^- in tap water. Thus, the content of NO_2^- that appears in all received food samples is followed by WHO regulations. While the

level of NO_2^- in tap water is higher than the regulation for drinking. It is clear that the developed method was available for NO_2^- determination in various samples and more cost-effectiveness and availability for the on–site applications, compared with a standard method.

Table 9 Recovery percentage of NO_2^- in real samples at various spiking concentrations measured with the proposed dual colorimetric and electrochemical sensor and validated with Griess Assay.

Samples	Spiked (mM)	This work			Griess Assay		
		Found (mM)	%Recovery	%RSD	Found (mM)	%Recovery	%RSD
Butter-head	0[a]	ND	-	-	ND	-	-
	0.1[a]	0.10±0.0050	100	4.7	0.10±0.0010	103	0.49
	0.2[a]	0.20±0.0060	101	2.9	0.21±0.0010	103	0.49
	0.3[a]	0.29±0.010	97	3.1	0.28±0.0020	92	0.73
	1[b]	1.0±0.0050	103	0.40	1.0±0.024	104	2.3
	2[b]	2.2±0.027	108	1.2	2.0±0.011	102	0.54
	4[b]	3.9±0.034	98	0.86	4.1±0.019	103	0.46
Green oak	0[a]	ND	-	-	ND	-	-
	0.1[a]	0.10±0.0010	100	1.3	0.10±0.002	106	1.7
	0.2[a]	0.21±0.0020	103	1.0	0.19±0.003	95	1.8
	0.3[a]	0.30±0.0010	98	0.34	0.32±0.005	107	1.6
	1[b]	1.0±0.0090	104	0.87	1.1±0.019	107	1.7
	2[b]	2.1±0.015	107	0.71	1.9±0.035	95	1.8
	4[b]	3.9±0.080	99	2.0	3.9±0.051	98	1.3
Red oak	0[a]	ND	-	-	ND	-	-
	0.1[a]	0.10±0.0048	101	4.8	0.094±0.0031	94	3.3
	0.2[a]	0.20±0.0033	101	1.6	0.20±0.0012	102	0.60
	0.3[a]	0.30±0.0013	101	0.43	0.29±0.011	96	3.7
	1[b]	1.06±0.0060	106	0.56	0.94±0.028	94	3.0
	2[b]	1.66±0.022	83	1.3	2.0±0.022	102	1.1
	4[b]	4.03±0.079	101	2.0	4.3±0.011	108	2.6
Salad cos	0[a]	ND	-	-	ND	-	-
	0.1[a]	0.10±0.000	101	0.10	0.11±0.002	105	2.08
	0.2[a]	0.20±0.0050	101	2.58	0.21±0.002	104	0.88
	0.3[a]	0.30±0.012	100	3.98	0.31±0.012	102	3.92
	1[b]	0.96±0.010	96	0.93	1.0±0.012	102	1.17
	2[b]	1.9±0.018	93	0.99	2.1±0.100	104	4.77
	4[b]	4.1±0.093	103	2.17	4.2±0.037	105	0.88

Samples	Spiked (mM)	This work			Griess Assay		
		Found (mM)	%Recovery	%RSD	Found (mM)	%Recovery	%RSD
Bologna	0[a]	0.13±0.00010	-	2.3	0.14±0.00020	-	0.36
	0.1[a]	0.23±0.0030	99	3.0	0.24±0.0030	105	1.2
	0.2[a]	0.34±0.0060	103	3.2	0.32±0.0020	96	0.66
	0.3[a]	0.44±0.0080	103	2.6	0.44±0.0030	101	0.60
	1[b]	1.2±0.0070	103	0.58	1.1±0.0050	97	0.45
	2[b]	1.9±0.028	96	1.3	2.1±0.013	100	0.63
	4[b]	4.3±0.049	103	1.2	4.4±0.11	106	2.6
Ham	0[a]	0.15±0.0010	-	3.6	0.15±0.0020	-	1.1
	0.1[a]	0.25±0.0020	101	15	0.24±0.0040	95	1.7
	0.2[a]	0.36±0.0040	102	2.2	0.35±0.0040	101	1.3
	0.3[a]	0.46±0.0050	103	1.7	0.44±0.0090	97	2.0
	1[b]	1.2±0.0080	104	0.67	1.2±0.045	103	3.8
	2[b]	2.2±0.014	101	0.64	2.2±0.072	102	3.3
	4[b]	4.3±0.17	103	3.8	4.4±0.18	105	4.1
Meat ball	0[a]	0.18±0.00011	-	2.8	0.17±0.0060	-	3.7
	0.1[a]	0.28±0.0020	104	1.8	0.25±0.0070	93	2.7
	0.2[a]	0.38±0.0030	102	1.6	0.37±0.014	99	3.8
	0.3[a]	0.48±0.0030	101	0.93	0.45±0.0070	96	1.6
	1[b]	1.20±0.010	102	0.80	1.1±0.011	96	0.85
	2[b]	2.1±0.018	98	0.82	2.2±0.014	102	0.65
	4[b]	4.1±0.042	99	1.0	4.2±0.066	100	1.6
Tap water	0[a]	0.045±0.00011	-	1.2	0.051±0.0020	-	4.7
	0.1[a]	0.15±0.001	102	0.88	0.15±0.0020	104	1.5
	0.2[a]	0.25±0.005	102	2..5	0.25±0.0060	101	2.5
	0.3[a]	0.34±0.010	99	3.3	0.34±0.0030	98	1.0
	1[b]	0.98±0.017	93	1.7	1.0±0.017	98	1.6
	2[b]	2.0±0.025	97	1.3	2.1±0.020	102	0.96
	4[b]	4.2±0.018	103	0.43	4.2±0.036	104	0.86
Soil	0[a]	ND	-	-	ND	-	-
	0.1[a]	0.10±0.0020	104	1.64	0.091±0.0020	91	1.7
	0.2[a]	0.20±0.0060	101	2.81	0.19±0.0020	94	1.3
	0.3[a]	0.30±0.011	101	3.50	0.29±0.0020	96	0.74
	1[b]	1.0±0.014	100	1.40	0.98±0.034	98	3.5
	2[b]	2.1±0.017	103	0.84	1.9±0.077	96	4.0
	4[b]	4.0±0.036	100	0.89	3.9±0.15	98	3.8

[a] The determination of NO_2^- performed by electrochemical detection.

[b] The determination of NO_2^-performed by colorimetric detection.

[c] ND = not detected.

CHAPTER V:

CONCLUSION

5.1 Conclusions

This work has developed a portable nitrite sensor with dual-detection mode using electrochemistry and colorimetry in a single device. For colorimetric detection of nitrite, making alternative redox-titration based on permanganometry more practical has been done on PADs to provide more concision, convenience, simplicity, and friendly use. Moreover, to reach a higher ability of detection in actual samples, the CA/SPCE with the electrochemical detection has been utilized together to solve the expectation which is appropriate for an expert chemist. The detection has been easily operated with a single introduction of a sample solution. With the fluidic properties of the proposed device, the sample solution could be flowed to the colorimetric pad and penetrated through the surface of the electrode simultaneously.

As a single method, colorimetric detection in the strong color sample, the color of samples that exhibit a similar shade of reagent color, interrupted the nitrite determination. The collaboration of color-independent and high-sensitivity methods like electrochemical detection has successfully solved this issue. With the electrochemical techniques, the requirement of specific skills and equipment are the limitations. The collaboration of the facile colorimetric method which is based on color perception by the naked eye, combined with a simple $KMnO_4$ reagent expands the availability of users and applications. Furthermore, the colorimetric pad can be utilized as a cut-off device to assign the overdose level of NO_2^- for consumption according to WHO standards in the determination of nitrite in consumption water.

The co-operation of dual mode on the proposed device not only offers benefits towards rapid response, cost-effectiveness, wider analytical linearity, and portability. But it is also expanding customer acquisition for both unskilled and well-

skilled users wherewith more facility of the proposed method, availability to approach a cost-effective reagent and common equipment.

Although the weakness in this dissertation is the poor stability of $KMnO_4$, a colorimetric reagent, the acidified reagent should be freshly prepared. However, it still is practical for field measurement by using appropriate packaging or containers with appropriate volume, which prevents light and oxygen from keeping the reagents.

5.2 Future perspectives

Firstly, due to the poor stability of the proposed colorimetric reagent, to improve stability, the $KMnO_4$ dye might be encapsulated on a zeolite nanostructure carrier with an acid-activating tailor-made capping unit. Alternatively, by modifying additional functional groups on an optional core transition metal. Moreover, as provided benefits of the proposed sensor, the dual mode detection design is feasible for adaptation of determination of other electroactive species.

REFERENCES

1. Shakil, M.H., et al., *Nitrites in Cured Meats, Health Risk Issues, Alternatives to Nitrites: A Review.* Foods, 2022. **11**(21): p. 3355.
2. Chazelas, E., et al., *Nitrites and nitrates from food additives and cancer risk: results from the NutriNet-Santé cohort.* European Journal of Public Health, 2021. **31**(Supplement_3): p. ckab165.244.
3. Bollag, J.-M. and N.M. Henninger, *Effects of nitrite toxicity on soil bacteria under aerobic and anaerobic conditions.* Soil Biology and Biochemistry, 1978. **10**(5): p. 377-381.
4. Hauck, R., *Nitrogen fertilizer effects on nitrogen cycle processes.* Ecological Bulletins, 1981. p. 551-562.
5. Zhou, N., et al., *The negative effects of the excessive nitrite accumulation raised by anaerobic bioaugmentation on bioremediation of PAH-contaminated soil.* Bioresource Technology, 2024. **393**: p. 130090.
6. Jensen, F.B., *Nitrite disrupts multiple physiological functions in aquatic animals.* Comparative Biochemistry and Physiology Part A: Molecular & Integrative Physiology, 2003. **135**(1): p. 9-24.
7. Kroupova, H., et al., *Effect of nitrite on early-life stages of common carp (Cyprinus carpio L.).* Environmental Toxicology and Chemistry, 2010. **29**(3): p. 535-540.
8. Debeuckelaere, W., R.P. Berbejal, and M.-A.G. Rosell, *Food additives, enzymes, and flavourings legislation in the European Union.* Food Additives and Packaging, 2014. p. 41-56.
9. Wolrd Health Organization (WHO), *Guidelines for drinking-water quality.* World Health Organization, 2011. **216**: p. 303–304.
10. Bratton, A.C. and E. Marshall Jr, *A new coupling component for sulfanilamide determination.* Journal of Biological Chemistry, 1939. **128**(2): p. 537-550.
11. Mesquita, R.B.R., et al., *Development of a sequential injection system for the determination of nitrite and nitrate in waters with different salinity: application to estuaries in NW Portugal.* Analytical Methods, 2009. **1**(3): p. 195-202.

12. Karali, K.K., L. Sygellou, and C.D. Stalikas, *Highly fluorescent N-doped carbon nanodots as an effective multi-probe quenching system for the determination of nitrite, nitrate and ferric ions in food matrices.* Talanta, 2018. **189**: p. 480-488.
13. Lin, K., et al., *An automated spectrophotometric method for the direct determination of nitrite and nitrate in seawater: Nitrite removal with sulfamic acid before nitrate reduction using the vanadium reduction method.* Microchemical Journal, 2020. **158**: p. 105272.
14. Wang, X., et al., *Fluorescence-based measurements for the determination of nitrite using a coumarin derivative sensor based on inner filter effect.* Analytical Methods, 2020. **12**(8): p. 1107-1114.
15. Ponhong, K., et al., *Dual determination of nitrite and iron by a single greener sequential injection spectrophotometric system employing a simple single aqueous extract from Areca catechu Linn. serving as a natural reagent.* RSC Advances, 2022. **12**(31): p. 20110-20121.
16. Bollenbach, A., E. Hanff, and D. Tsikas, *Investigation of NG-hydroxy-l-arginine interference in the quantitative determination of nitrite and nitrate in human plasma and urine by GC-NICI-MS.* Journal of Chromatography B, 2018. **1100-1101**: p. 174-178.
17. Zhang, S.-X., et al., *A high-throughput headspace gas chromatographic technique for the determination of nitrite content in water samples.* Journal of Chromatography A, 2018. **1538**: p. 104-107.
18. D'Amore, T., et al., *Development and Validation of an Analytical Method for Nitrite and Nitrate Determination in Meat Products by Capillary Ion Chromatography (CIC).* Food Analytical Methods, 2019. **12**(8): p. 1813-1822.
19. Lin, S.-L., J.-W. Hsu, and M.-R. Fuh, *Simultaneous determination of nitrate and nitrite in vegetables by poly (vinylimidazole-co-ethylene dimethacrylate) monolithic capillary liquid chromatography with UV detection.* Talanta, 2019. **205**: p. 120082.
20. Coviello, D., et al., *Validation of an analytical method for nitrite and nitrate determination in meat foods for infants by ion chromatography with conductivity detection.* Foods, 2020. **9**(9): p. 1238.

21. Guan, F., H. Wu, and Y. Luo, *Sensitive and selective method for direct determination of nitrite and nitrate by high-performance capillary electrophoresis.* Journal of Chromatography A, 1996. **719**(2): p. 427-433.

22. Fuiko, R., et al., *Capillary electrophoresis for continuous nitrogen quantification in wastewater treatment processes.* Talanta, 2019. **195**: p. 366-371.

23. Moravský, L., et al., *Determination of nitrites and nitrates in plasma-activated deionized water by microchip capillary electrophoresis.* Contributions to Plasma Physics, 2020. **60**(7): p. e202000014.

24. Tembo, Z.N. and S.F. Aygun, *Capillary electrophoretic method for the simultaneous determination of nitrate, nitrite and bromate ions in some selected plants.* Journal of the Science of Food and Agriculture, 2021. **101**(13): p. 5391-5397.

25. Griess, P., *Bemerkungen zu der Abhandlung der HH. Weselsky und Benedikt " Ueber einige Azoverbindungen".* Berichte der deutschen chemischen Gesellschaft, 1879. **12**(1): p. 426-428.

26. Stein, L.Y. and M.G. Klotz, *The nitrogen cycle.* Current Biology, 2016. **26**(3): p. R94-R98.

27. Cole, J. and C. Brown, *Nitrite reduction to ammonia by fermentative bacteria: a short circuit in the biological nitrogen cycle.* FEMS Microbiology Letters, 1980. **7**(2): p. 65-72.

28. Helmestine, A. *Nitrogen Cycle*. 2023 30 August 2023 [cited 2024 7 March]; Available from: https://sciencenotes.org/nitrogen-cycle/.

29. Fernandes, G.M., et al., *Novel approaches for colorimetric measurements in analytical chemistry–A review.* Analytica Chimica Acta, 2020. **1135**: p. 187-203.

30. Swinehart, D.F., *The beer-lambert law.* Journal of chemical education, 1962. **39**(7): p. 333.

31. Cate, D.M., et al., *Recent Developments in Paper-Based Microfluidic Devices.* Analytical Chemistry, 2015. **87**(1): p. 19-41.

32. Sumriddetchkajorn, S., K. Chaitavon, and Y. Intaravanne, *Mobile-platform based colorimeter for monitoring chlorine concentration in water.* Sensors and Actuators B: Chemical, 2014. **191**: p. 561-566.
33. de Oliveira, H.J.S., et al., *A handheld smartphone-controlled spectrophotometer based on hue to wavelength conversion for molecular absorption and emission measurements.* Sensors and Actuators B: Chemical, 2017. **238**: p. 1084-1091.
34. Ra, M., et al., *Smartphone-based point-of-care urinalysis under variable illumination.* IEEE journal of translational engineering in health and medicine, 2017. **6**: p. 1-11.
35. *Commission internationale de l'Eclairage* (CIE), *Commission internationale de l'Eclairage proceedings*, Cambridge: Cambridge University Press, 1931.
36. Smith, T. and J. Guild, *The CIE colorimetric standards and their use.* Transactions of the optical society, 1931. **33**(3): p. 73.
37. Weeks, A.R., L.J. Sartor, and H.R. Myler, *Histogram specification of 24-bit color images in the color difference (CY) color space.* Journal of electronic imaging, 1999. **8**(3): p. 290-300.
38. Woolf, M.S., et al., *Digital postprocessing and image segmentation for objective analysis of colorimetric reactions.* Nature protocols, 2021. **16**(1): p. 218-238.
39. Bard, A.J., L.R. Faulkner, and H.S. White, *Electrochemical methods: fundamentals and applications*. John Wiley & Sons, 2022.
40. Langhus, D.L., *Analytical Electrochemistry (Wang, Joseph)*, ACS Publications, 2001.
41. Wang, J., Analytical Electrochemistry. 2006. p. 1-28.
42. Skoog, D.A., et al., *Fundamentals of analytical chemistry*. Cengage learning, 2013.
43. Harris, D.C. and C.A. Lucy, *Quantitative chemical analysis*. Tenth edition ed. Austin: Macmillan Learning Austin, 2020.
44. Peng, P., et al., *Bioinspired ionic control for energy and information flow.* International Journal of Smart and Nano Materials. 2024. 15(1) p. 198-221.
45. Liu, J., et al., *Application and Progress of Chemometrics in Voltammetric Biosensing.* Biosensors, 2022. **12**(7): p. 494.
46. Bracher, C. *Cyclic Voltammetry Basic Principles, Theory and Setup*. 2022. [cited 2024-03-07]; Available from: https://www.ossila.com/pages/cyclic-voltammetry.

47. PalmSens. *Differential Pulse Voltammetry (DPV)*. 2021. [cited 2024-03-07]; Available from: https://www.palmsens.com/knowledgebase-article/differential-pulse-voltammetry-dpv.

48. Jaiswal, N. and I. Tiwari, *Recent build outs in electroanalytical biosensors based on carbon-nanomaterial modified screen printed electrode platforms.* Analytical Methods, 2017. **9**(26): p. 3895-3907.

49. Metters, J.P., R.O. Kadara, and C.E. Banks, *New directions in screen printed electroanalytical sensors: an overview of recent developments.* Analyst, 2011. **136**(6): p. 1067-1076.

50. Friuli, M., et al., *Cellulose Acetate and Cardanol Based Seed Coating for Intraspecific Weeding Coupled with Natural Herbicide Spraying.* Journal of Polymers and the Environment, 2020. **28**(11): p. 2893-2904.

51. Wang, J., T. Golden, and R. Li, *Cobalt phthalocyanine/cellulose acetate chemically modified electrodes for electrochemical detection in flowing streams. Multifunctional operation based upon the coupling of electrocatalysis and permselectivity.* Analytical chemistry, 1988. **60**(15): p. 1642-1645.

52. Wu, S., et al., *Stability improvement of prussian blue by a protective cellulose acetate membrane for hydrogen peroxide sensing in neutral media.* Electroanalysis, 2010. **22**(16): p. 1906-1910.

53. Arakawa, T., et al., *A Wearable Cellulose Acetate-Coated Mouthguard Biosensor for In Vivo Salivary Glucose Measurement.* Analytical Chemistry, 2020. **92**(18): p. 12201-12207.

54. Xu, Y., Q. Hao, and D. Mandler, *Electrochemical detection of dopamine by a calixarene-cellulose acetate mixed Langmuir-Blodgett monolayer.* Analytica Chimica Acta, 2018. **1042**: p. 29-36.

55. Gobalu, K., et al., *Molybdenum disulphide/cellulose acetate nanofiber composite on screen printed electrodes for detecting cardiac troponin by electrical impedance spectroscopy.* Cellulose, 2021. **28**(9): p. 5761-5774.

56. Vasudevan, M., et al., *Cellulose acetate-MoS2 nanopetal hybrid: A highly sensitive and selective electrochemical aptasensor of Troponin I for the early*

diagnosis of Acute Myocardial Infarction. Journal of the Taiwan Institute of Chemical Engineers, 2021. **118**: p. 245-253.

57. El-Moghazy, A.Y., et al., *A signal-on electrochemical aptasensor based on silanized cellulose nanofibers for rapid point-of-use detection of ochratoxin A.* Microchimica Acta, 2020. **187**(9): p. 535.
58. Casella, I.G., D. Gioia, and M. Rutilo, *A multi-walled carbon nanotubes/cellulose acetate composite electrode (MWCNT/CA) as sensing probe for the amperometric determination of some catecholamines.* Sensors and Actuators B: Chemical, 2018. **255**: p. 3533-3540.
59. Badea, M., et al., *New electrochemical sensors for detection of nitrites and nitrates.* Journal of Electroanalytical Chemistry, 2001. **509**(1): p. 66-72.
60. Tsikas, D., *Analysis of nitrite and nitrate in biological fluids by assays based on the Griess reaction: appraisal of the Griess reaction in the L-arginine/nitric oxide area of research.* J Chromatogr B Analyt Technol Biomed Life Sci, 2007. **851**(1-2): p. 51-70.
61. Nilghaz, A., et al., *Semiquantitative analysis on microfluidic thread-based analytical devices by ruler.* Sensors and Actuators B: Chemical, 2014. **191**: p. 586-594.
62. Wicaksono, D.H.B., et al., *Cotton fiber-based assay with time-based microfluidic absorption sampling for point-of-care applications.* Bioanalysis, 2019. **11**(9): p. 855-873.
63. Nilghaz, A., et al., *Multiple semi-quantitative colorimetric assays in compact embeddable microfluidic cloth-based analytical device (μ-CAD) for effective point-of-care diagnostic.* Microfluidics and Nanofluidics, 2015. **19**(2): p. 317-333.
64. Jayawardane, B.M., et al., *Microfluidic Paper-Based Analytical Device for the Determination of Nitrite and Nitrate.* Analytical Chemistry, 2014. **86**(15): p. 7274-7279.
65. Bhakta, S.A., et al., *Determination of nitrite in saliva using microfluidic paper-based analytical devices.* Analytica Chimica Acta, 2014. **809**: p. 117-122.

66. Nalin, R. and D. Wijitar, *Paper-based Analytical Device (PAD) for the Determination of Borax, Salicylic Acid, Nitrite, and Nitrate by Colorimetric Methods.* Journal of Analytical Chemistry, 2020. **75**(4): p. 487-494.

67. Thongkam, T. and K. Hemavibool, *An environmentally friendly microfluidic paper-based analytical device for simultaneous colorimetric detection of nitrite and nitrate in food products.* Microchemical Journal, 2020. **159**: p. 105412.

68. Singh, P., et al., *A review on spectroscopic methods for determination of nitrite and nitrate in environmental samples.* Talanta, 2019. **191**: p. 364-381.

69. Singhaphan, P. and F. Unob, *Thread-based platform for nitrite detection based on a modified Griess assay.* Sensors and Actuators B: Chemical, 2021. **327**: p. 128938.

70. Murthy, P.C.A., M. F. S.; Ashok, D., *"Redox titration: I" in University Chemistry*. New Dehli: new age international(P) limited 2022. **1**. p. 634-637

71. Bray, W.C. and H.E. Miller, *The standardization of thiosulfate solution by the permanganate-iodide and dichromate-iodide and dichromate-iodide methods.* Journal of the American Chemical Society, 1924. **46**(10): p. 2204-2211.

72. Fowler, R.M., *Standardization of permanganate solutions with sodium oxalate.* Journal of Research of the National Bureau of Standards, 1935. **15**.

73. Bowman, M.I., *The reaction between potassium permanganate and hydrogen peroxide.* Journal of Chemical Education, 1949. **26**(2): p. 103.

74. Dikshitulu, L.S.A. and G.G. Rao, *Titrimetric determination of vanadium (IV) with potassium permanganate at the room temperature, using phosphoric acid as catalyst and ferroin as internal indicator.* Fresenius' Zeitschrift für analytische Chemie, 1962. **189**(5): p. 421-426.

75. Dózsa, L. and M.T. Beck, *The mechanism of the permanganate-nitrite reaction.* Inorganica Chimica Acta, 1970. **4**: p. 219-225.

76. Kaufman, S. and H. Devoe, *Iron analysis by redox titration: A general chemistry experiment.* Journal of Chemical Education, 1988. **65**(2): p. 183.

77. Kozub, B.R., N.V. Rees, and R.G. Compton, *Electrochemical determination of nitrite at a bare glassy carbon electrode; why chemically modify electrodes?* Sensors and Actuators B: Chemical, 2010. **143**(2): p. 539-546.

78. Uslu, B. and S.A. Ozkan, *Electroanalytical Application of Carbon Based Electrodes to the Pharmaceuticals.* Analytical Letters, 2007. **40**(5): p. 817-853.

79. Xiao, Q., et al., *The graphene/polypyrrole/chitosan-modified glassy carbon electrode for electrochemical nitrite detection.* Ionics, 2018. **24**(3): p. 845-859.

80. Fan, Z., et al., *Preparation of manganese porphyrin/niobium tungstate nanocomposites for enhanced electrochemical detection of nitrite.* Journal of Materials Science, 2019. **54**(14): p. 10204-10216.

81. Sun, C., et al., *An electrochemical sensor for nitrite using a glassy carbon electrode modified with Cu/CBSA nanoflower networks.* Analytical Methods, 2019. **11**(39): p. 4998-5006.

82. Sahoo, S., et al., *Interfacial polymerized RGO/MnFe2O4/polyaniline fibrous nanocomposite supported glassy carbon electrode for selective and ultrasensitive detection of nitrite.* Sensors and Actuators B: Chemical, 2020. **309**: p. 127763.

83. Mounesh and K.R. Venugopala Reddy, *Sensitive and reliable electrochemical detection of nitrite and H2O2 embellish-CoPc coupled with appliance of composite MWCNTs.* Analytica Chimica Acta, 2020. **1108**: p. 98-107.

84. Ding, F., et al., *A Metal–Organic Gel-Carbon Nanotube Nanocomposite for Electrochemical Detection of Nitrite.* ACS Applied Electronic Materials, 2021. **3**(2): p. 761-768.

85. Talbi, M., et al., *Enhanced Nitrite Detection by a Carbon Screen Printed Electrode Modified with Photochemically-Made AuNPs.* Chemosensors, 2022. **10**(2).

86. Yılmaz-Alhan, B., et al., *Determination of nitrite on manganese dioxide doped reduced graphene oxide modified glassy carbon by differential pulse voltammetry.* Chemical Papers, 2022. **76**(8): p. 4919-4925.

87. Wang, M., et al., *Coupling diazotization with oxidase-mimetic catalysis to realize dual-mode double-ratiometric colorimetric and electrochemical sensing of nitrite.* Sensors and Actuators B: Chemical, 2022. **355**: p. 131308.

88. Rodríguez, F., et al., *Preparation, characterization, and adsorption properties of cellulose acetate-polyaniline membranes.* Journal of Applied Polymer Science, 2009. **111**(3): p. 1216-1224.

89. Vanjari, S.R.K., et al., *Bufferless lysis of erythrocytes for isolation of hemoglobin using modified cellulose acetate membranes.* Biotechnology and Bioprocess Engineering, 2012. **17**(2): p. 309-315.

90. Varga, B., et al., *Design and Optimization of Laccase Immobilization in Cellulose Acetate Microfiltration Membrane for Micropollutant Remediation.* Catalysts, 2023. **13**(2): p. 222.

91. Sudiarti, T., et al., *Mechanical strength and ionic conductivity of polymer electrolyte membranes prepared from cellulose acetate-lithium perchlorate.* IOP Conference Series: Materials Science and Engineering, 2017. **223**(1): p. 012052.

92. Santos-Sauceda, I., et al., *Electrospun cellulose acetate fibers for the photodecolorization of methylene blue solutions under natural sunlight.* Polymer Bulletin, 2021. **78**(8): p. 4419-4438.

93. Kunpatee, K., et al., *Electrochemical lateral flow immunosensor with enhanced reproducibility for milk allergen detection.* Sensors and Actuators B: Chemical, 2024. **401**: p. 135042.

94. Wang, Y., E. Laborda, and R.G. Compton, *Electrochemical oxidation of nitrite: Kinetic, mechanistic and analytical study by square wave voltammetry.* Journal of Electroanalytical Chemistry, 2012. **670**: p. 56-61.

95. Wilbrandt, W., *The significance of the structure of a membrane for its selective permeability.* The Journal of General Physiology, 1935. **18**(6): p. 933-965.

96. Pinyorospathum, C., et al., *A fabrication of cost-effective paper-based colorimetric devices for nitrite detection.* Science, Engineering and Health Studies, 2022. **16**: p. 22020013.

97. Hurvich, L.M. and D. Jameson, *An opponent-process theory of color vision.* Psychological review, 1957. **64**(6p1): p. 384.

มหาวิทยาลัยศิลปากร

VITA

NAME	Miss Parima Tiawpisitpong
INSTITUTIONS ATTENDED	B.Sc. (Chemistry), Silpakorn University
PUBLICATION	Pinyorospathum C., Choeychit J., Tiawpisitpong P., Charoenkitamorn K.* (2022), A Fabrication of Cost-effective Paper-based Colorimetric Devices for Nitrite Detection, Science, Engineering and Health Studies, 16, 22020013. (ISI, Scopus). Tiawpisitpong P., Pinyorospathum C., Charoenkitamorn K. (2023) "Dual-mode portable sensor using colorimetry and electrochemistry for nitrite detection" Proceedings of the 16th EURASIA Conference on chemical science 2023 (EuAsC2S-16), Bangkok, Thailand, December 13-15, pp.183-188.
AWARD RECEIVED	-